Rotating Disk and Ring–Disk Electrodes

S Vesztergom, Eötvös Loránd University, Budapest, Hungary

Introduction

Electrochemical techniques involving the use of electrodes that move with respect to the solution are commonly termed hydrodynamic techniques. These include configurations where the electrolyte solution is in motion while the electrode itself is stagnant (such as in channel flow systems) or ones where the electrode itself is moved in an otherwise quiescent liquid phase. The most common example of hydrodynamic systems of the latter type is the rotating disk electrode (RDE) or its several variations such as the rotating ring–disk electrode (RRDE).

The advantage of all hydrodynamic methods, irrespective of the actual configuration, is that in such systems steady state can be attained rather quickly and stationary current/potential characteristics can be measured. Also, the rate of mass transfer in a hydrodynamic configuration is typically higher than that of diffusion alone in nonhydrodynamic systems and this makes the application of hydrodynamic methods extremely expedient, for example, in electrocatalysis research.

Although many hydrodynamic techniques were described in the literature—the first notion about that "movement" has a strong effect on currents measurable during electrolysis was made by Helmholtz[1] as early as 1880—the most convenient and widely used system is still the RDE, first described by Levich in 1944.[2] (Publication in English followed in 1947.[3]) This electrode is amenable to rigorous theoretical treatment and is easy to construct with a variety of electrode materials.

In what follows I give a brief overview of the most often used hydrodynamic systems: rotating disk and ring–disk electrodes.

As I intended this article to serve as a survey of rotating electrode methods, I did not extend its focus to every detail; however I did wish to highlight some practical aspects that remain unmentioned in other sources. The first part of this article (section "**Design**") is thus dedicated to the design of RDEs and RRDEs, as well as to experimental know-how. The basic principles of measurements as well as data analysis strategies are discussed first for RDEs (section "**Measurements With RDEs**"), then for RRDEs (section "**Measurements With RRDEs**").

Theory underlying the use of rotating electrodes is described in the section "**Theory**." Section "**Fluid Flow Under a Rotating Disk**" contains a description of the hydrodynamics of rotating disk systems, and goes more into details compared to most electrochemistry textbooks. In section "**Stationary Concentration Profiles and Currents at RDEs**," basic analytical expressions (such as the Levich and Koutecký–Levich equations) are derived for RDEs, and I intended this section to be a theoretical supplement to what was said in the section "**RDEs and RRDEs—Practical Aspects**."

Finally, section "**Digital Simulation of the RRDE System**" is dedicated to the theory of the RRDE systems. As from a mathematical point of view RRDEs are generally more complicated than RDEs, my intention in this section was not to derive analytical formulae but rather to demonstrate the use of numerical simulation techniques that can be used for the accurate modeling of RRDE experiments.

For a more detailed introduction to rotating electrode systems, I refer the reader to the electrochemistry textbook of Bard and Faulkner.[4] For readers who wish for an in-depth understanding, I recommend the famous textbook of Levich[5] or the excellent review of Gregory and Riddiford[6] on RDEs, as well as the handbook of Albery and Hitchman[7] on RRDEs. With respect to the topic of RRDEs, also the papers authored by Albery and his coworkers, which appeared over the 24 years between 1966 and 1989 on the columns of the Transactions of the Faraday Society, are recommended sources.[8–31]

RDEs and RRDEs—Practical Aspects

Design

RDEs and RRDEs owe their popularity to their very simple design. RDEs and RRDEs are commercially available, and are both relatively simple to construct.

In an RDE, the electrode material (usually some metal or glassy carbon, etc.) is embedded in a rod of insulating material such as Teflon or polyether ether ketone, as shown in Fig. 1. The construction of RRDEs, as also shown in Fig. 1, is slightly more complicated since in this case a second (ring) electrode material is also applied. The material of the ring can differ from that of the disk: it is however important that the ring should surround the disk electrode concentrically. The gap between the ring and disk materials should be filled by an insulator: usually but not necessarily, the gap is filled with the same material as that of the outer isolating mantle.

Measurements using conventional RDE or RRDE systems are usually carried out in an electrochemical cell similar to that shown in Fig. 2. For accurate measurements it is required that the plane of rotation is aligned horizontally and a large enough cell space is provided so that the natural convection profile remains undisturbed and no turbulence or vortices occur. It is also important to avoid leakage of the solution between the isolating mantle and the electrode material(s).[6] This necessitates careful construction, especially in the case of RRDEs.

As cells used for RDE or RRDE studies can usually not be made air-tight, measures must be taken to deaerate the solution thoroughly and to maintain an inert gas blanket over the solution for the time of the experiment, whenever oxygen-free conditions are required. Bubbling gas through the solution during the time of measurement is to be avoided, as this can disturb the convection profile of the rotating electrode.

RDEs and RRDEs are usually rotated at a given rate by a motor that is equipped with a tachometer and a precise control unit. Rotation rate is often denoted by f and is usually expressed in a unit of revolution per minute (min^{-1} or rpm). In practice, rotation rates used in RDE and RRDE studies vary between 100 and 3000 min^{-1}. In the mathematical description of RDE systems the angular frequency ω is more often used to express the speed of rotation. The two quantities are related by $\omega = 2\pi f$ and the angular frequency ω is usually given in units of hertz (Hz) or s^{-1}.

Most rotators available on the market can be used both with RDEs and with RRDEs: in the latter case, the rotator provides two separated electrical contacts, one for the disk and another for the ring electrode. Between the fixed and moving parts of the rotator units, electrical contact is usually provided either by carbon brushes or by mercury slip rings. Mercury contacts exhibit lower resistance and are less prone to noise than carbon brushes; however environmental and health hazards must be considered when using mercury-containing rotators. Such rotators are, for obvious reasons, not user-serviceable (and generally do not even require regular maintenance). On the other hand, carbon brush rotators do require maintenance, which involves the regular cleaning of the metallic commutators of the rotating shaft (parts which are contacted by the carbon brushes) by a cloth wetted with isopropanol, and the scheduled replacement of worn-out carbon brushes. Note that new carbon brushes need to be broken in (by rotation lasting

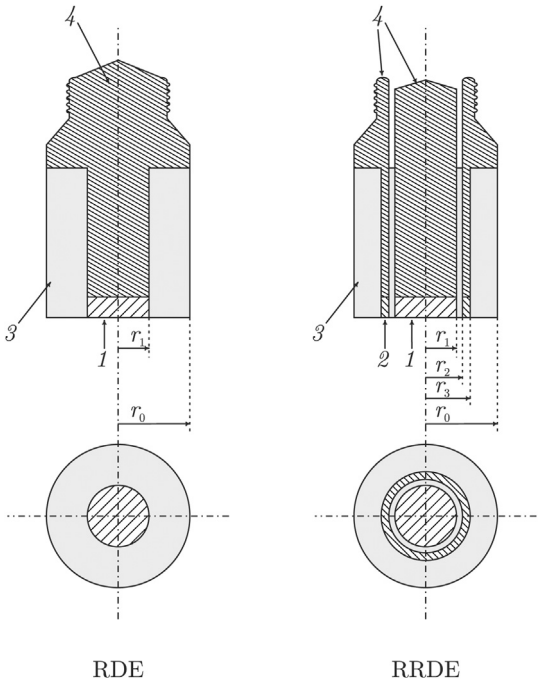

Fig. 1 Sketch of a rotating disk (RDE) and a rotating ring–disk electrode (RRDE) tip. Parts of the electrode tips—*1*: disk electrode material; *2*: ring electrode material; *3*: insulator; *4*: metal support. Dimensions—r_1: disk radius; r_2: inner ring radius; r_3: outer ring radius; r_0: overall radius of the tip.

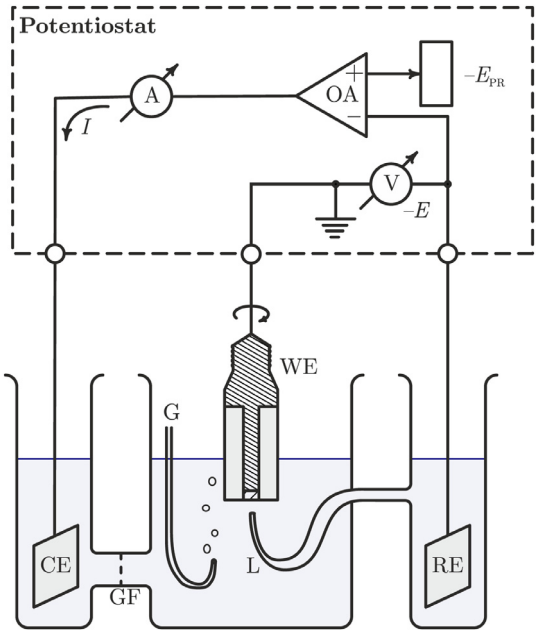

Fig. 2 Scheme of an electrochemical cell with a rotating disk electrode controlled by a simplified potentiostat circuit. Parts of the cell—*WE*, working electrode (RDE); *CE*, counter electrode; *RE*, reference electrode; *L*, Luggin capillary; *GF*, glass frit separating the counter and working electrode compartments; *G*, gas inlet. Parts of the potentiostat—*OA*, operational amplifier that keeps the potential of RE *vs.* WE (that is, $-E$) at a constant set-point level $-E_{PR}$ by passing a current *I* through the WE–CE loop. *A and V*, current and voltage meters.

a few hours) to assure good contact to the shaft. In case an RDE or RRDE measurement seems noisy, checking the carbon brushes should always be the first step of trouble-shooting.

Measurements With RDEs

RDE experiments do not substantially differ from any other electrochemical studies that involve a standard three-electrode cell (Fig. 2), except that with RDEs, different rotation rates can be set and the dependence of current on rotation rate can be analyzed. As opposed to quiescent systems, RDEs facilitate the measurement of truly stationary polarization curves; however they can also be used for the application of transient techniques such as linear sweep voltammetry.

For electrochemical systems where mass transfer (the diffusion of dissolved species) does not play any prominent role in determining the measurable current/voltage characteristics, the response measurable on an RDE should be very similar to that detected on stagnant electrodes. An example is shown in Fig. 3, exhibiting only slight differences between the cyclic voltammograms of the Au(poly) | H_2SO_4(aq) system, measured when the electrode is stagnant (curve *1*) and when it is rotated (curve *2*).

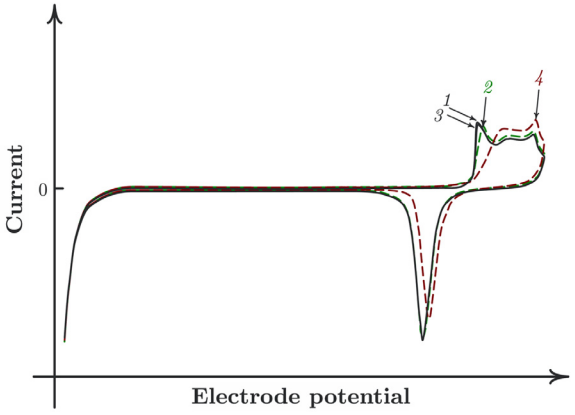

Fig. 3 Cyclic voltammograms (already attained their final shapes) of a polycrystalline gold disk immersed into a 0.5 mol dm^{-3} solution of sulfuric acid, recorded at a sweep rate of 50 mV s^{-1}. Curve *1* was measured on a nonrotating electrode; curve *2* was measured when the electrode was rotated at 500 min^{-1}. Curve *3*, which is almost fully overlapping with curve *1* at the present scale, was measured again on a nonrotating electrode, however following the addition of trace amounts of a chloride-containing contaminant. Curve *4* was recorded in the contaminated cell at 500 min^{-1}.

That rotation has practically no effect on this system is in fact not surprising, since the oxidation and the corresponding reduction of a gold surface should not be limited by the mass transfer of any species dissolved in the solution. Nevertheless, introducing rotation can still be expedient in order to check the purity of the system: this is because when differences between the response of stagnant and rotating electrodes do emerge, these often originate from an impurity of the solution.

As also shown in Fig. 3, by adding a very small amount of a chloride-containing contaminant to the solution, differences between the voltammetric response of rotating and stagnant electrodes become pronounced. In case of the Au(poly) | H_2SO_4(aq) system, the cause of this effect is the adsorption of chloride at the electrode surface which hinders its oxidation. As the surface coverage of Cl^- ions does depend on the concentration of chloride in the near-electrode solution layer, whether convection can resupply chloride has a deep impact on the measured cyclic voltammograms (CVs). This carries an important practical message for experimenters using hydrodynamic techniques: which is that the utilization of convection always makes sure that impurities, *whenever present in the system*, always end up at the electrode surface, and thus hydrodynamic measurements are often more sensitive to contaminations compared to other electrochemical techniques.

To this statement I add that in convective systems it is also more likely that products of the counter electrode reaction can reach the working electrode surface: therefore, separation of the counter and working electrode compartments (as was shown in Fig. 2) is essential.

Most RDE studies focus however not on surface-confined reactions but instead on electrode processes that involve dissolved reactants. In this case fluid flow is rather beneficial as it can provide a continuous supply of the reactants and as a result, on an RDE much larger faradaic currents can be upheld than on stagnant electrodes. In an RDE system, convection also makes sure that the products of the electrode reaction are swept away from the disk surface rather quickly. Consequently, reversal techniques common for quiescent systems—such as CV—are rarely applied to RDEs, although they can very well be used to demonstrate the effect of convection. This is shown by the CVs of Fig. 4, taken at different sweep and rotation rates in a system that contains an oxidized species which can undergo a reversible one-electron reduction.

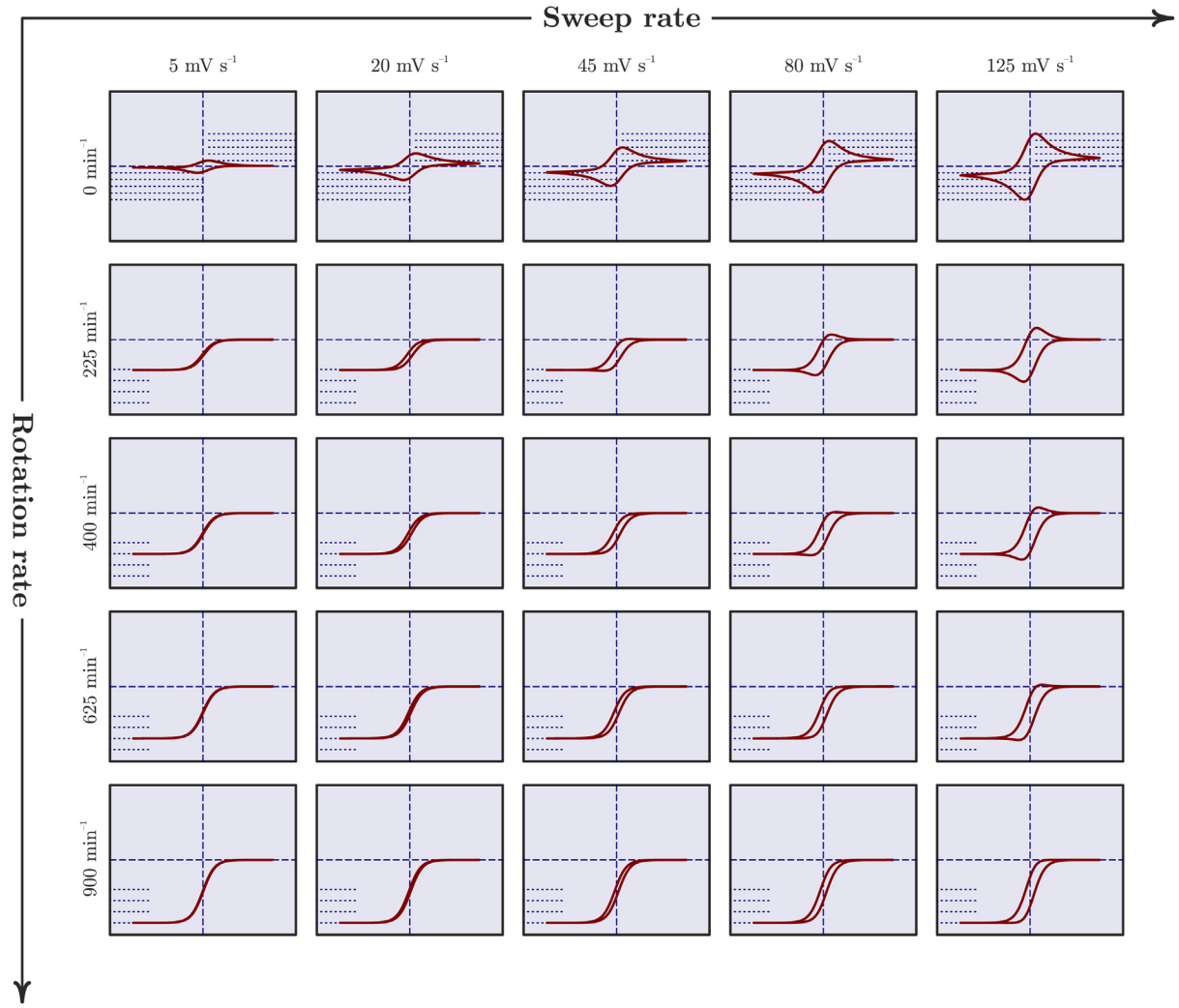

Fig. 4 Cyclic voltammograms (already attained their final shapes) of a disk electrode that is immersed into a solution containing an oxidized species that can undergo a fully reversible 1-electron reduction in which a reduced species is formed. CVs are recorded at different sweep and rotation rates. Initially, only the oxidized species are present in the cell.

In Fig. 4 it is apparent that in a quiescent system (i.e., at 0 min^{-1}) a reduction wave and a (reversal) oxidation wave are both present in the CVs and that the peak heights scale linearly with the square root of the sweep rate. On rotated electrodes, however (particularly if the rotation rate is high and the sweep rate is low), the reversal peak vanishes.

Also the cathodic scans of the CVs differ for rotated and quiescent systems in Fig. 4. At high rotation and relatively low sweep rates, the peak-like feature of the cathodic scans gets suppressed, as the cathodic current—instead of following a slow decay—attains a finite limit. As can be observed in Fig. 4, this "limiting current" is proportional to the square root of the rotation rate, and is described as

$$I_\ell = 0.620nFAD^{2/3}\nu^{-1/6}c_\infty\omega^{1/2}. \quad (1)$$

In Eq. (1), n is the number of electrons transferred in the reaction, $F = 96485.3$ C mol^{-1} is Faraday's constant, A is the surface area of the electrode, ν is the kinematic viscosity of the solution, c_∞ is the bulk concentration of the reacting species, and ω is the angular frequency of rotation. Eq. (1), the famous Levich-equation, is central to rotating disk systems. (Insight to the theoretical background of the important equations used for the analysis of RDE measurements—such as the Levich equation, Eq. (1) and the Koutecký–Levich equation, Eq. (4)—is given in the section "Theory.")

Although the Levich equation contains only two parameters directly related to the interface—the area of the electrode A and the number of electrons transferred in the electrode reaction n—, and thus it has little to say about the kinetics of the electrode reaction, it still offers a straightforward way for determining bulk parameters of the system. For example, if both A and n, as well as the bulk concentration of the reacting species c_∞ and the kinematic viscosity ν of the electrolyte solution are known, the measurement of limiting currents and their analysis based on the Levich equation can be used for determining the diffusion coefficient D of the reacting species.

In order to use the Levich equation for the determination of diffusion coefficients, the dependence of the limiting current versus the square root of the rotation rate is to be analyzed. An example is given in Fig. 5A, showing stationary polarization curves measured at different rotation rates in a system that contains an oxidized species undergoing reduction at certain (cathodic) potentials.

For valid analysis, care must be taken during such measurements as to that the polarization curves are truly *stationary*. This can be achieved either by setting the potential point-by-point, and then determining a constant current corresponding to each potential value or by recording linear sweep voltammograms at different (preferably low) sweep rates and ruling out any sweep rate dependence.

It is apparent in Fig. 5A that at not very cathodic potentials (i.e., within the regime of "kinetic control") the measured current strongly increases with the applied cathodic potential. As the potential is set to more cathodic values, the current increase breaks down and after passing a regime of "mixed control," current attains a limiting value that is already "transport controlled"— see the approximate control regime boundaries marked on the colored stripe in Fig. 5A.

The underlying physical picture is that at not very negative potentials, the rate of the reaction (i.e., the probability of that an oxidized species near the electrode surface can undergo a reduction event) is relatively small; however it increases with the applied potential. The current versus potential dependence within this "kinetic control" regime is essentially determined by the mechanism

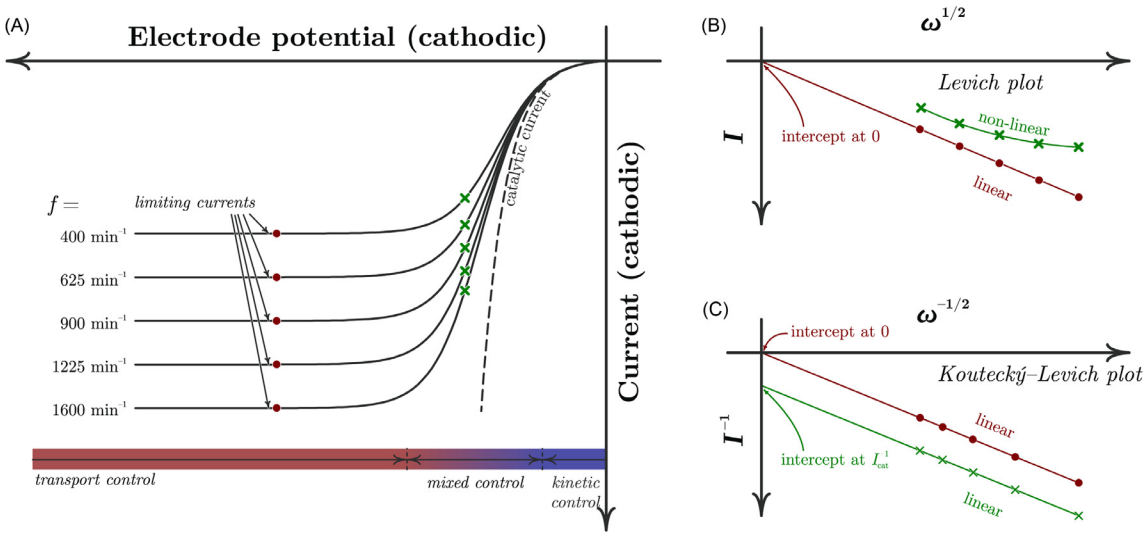

Fig. 5 (A) Stationary polarization curves measured at different rotation rates for a system where an oxidized species (of finite bulk concentration) undergoes reduction at a rotating disk electrode. Selected current values (marked by *red dots* and *green crosses*) are plotted on a Levich (B) and on a Koutecký–Levich (C) plot.

of the electrode reaction. In the simplest case one can assume that current depends exponentially on the applied potential, as is described by the Erdey-Grúz–Volmer–Butler equation:

$$I = nFAkc_0 \exp\left[-\frac{\alpha nF}{RT}\left(E - E_{eq}\right)\right], \tag{2}$$

where $(E - E_{eq})$ is the overpotential (the difference of the electrode potential E and its equilibrium value E_{eq}, often denoted as η), α is the charge transfer coefficient, k is the rate coefficient, and c_0 is the concentration of the reactant *at the electrode surface*.

In a system where the *bulk* concentration of the reactant (c_∞) is large enough so that the electrode reaction cannot cause any significant near-surface concentration decrease (that is, $c_0 \approx c_\infty$), the measured current practically coincides with a so-called catalytic current that can be obtained by assuming that $c_0 = c_\infty$ in Eq. (2), and thus

$$I_{cat} = nFAkc_\infty \exp\left(-\frac{\alpha nF\eta}{RT}\right). \tag{3}$$

The situation is however different for systems where the bulk concentration c_∞ of the reacting species is not infinitely high. In such systems, as shown in Fig. 5A, the measured polarization curves follow the catalytic current only at low overpotentials. As the overpotential is set to higher values, the driving force of the electrode reaction becomes so large that practically every oxidized molecule reaching the electrode surface immediately undergoes reduction. In this case increasing further the overpotential has already no effect on the measured current, as the rate of the reaction is already "transport controlled"—that is, the reaction rate is limited by the speed at which new reactant species are transported from inside the bulk to the electrode surface, and not by the (practically infinite) rate of the electrode reaction. Naturally, at certain overpotentials both kinetic and transport control have a role in determining current; thus there exists also a "mixed control" regime between the regimes of kinetic and transport control (see Fig. 5A).

In order to use the Levich equation (Eq. 1) for the determination of bulk transport parameters, limiting current sections must be attained at all rotation rates. In a practical system, these can be recognized as flat plateaus of the polarization curves; that is, sections where $dI/dE \approx 0$. By reading the currents at the plateau sections (see the red dots in Fig. 5A) and plotting them as a function of the square root of the angular frequency of rotation ($\sqrt{\omega}$), one should obtain a straight line with an intercept of zero, as in Fig. 5B (red dots and line). The slope of this line (commonly called the "Levich slope") can then be estimated and used, for example, for calculating the diffusion coefficient of the reacting species from Eq. (1).

In some practical systems, however, the measurement of true limiting currents is not feasible, either due to instrumental limitations, due to gas evolution (resulting in noisy curves), or due to the fact that the electrochemical stability window of the system is not broad enough. In the latter case, the onset of additional currents makes the limiting current plateaus ill-defined.

Assume, for example, that the polarization curves of Fig. 5A can only be experimentally determined up to the potentials marked by the green crosses, and that the limiting current sections (for whatever reason) cannot be reached. If we wrongly identify the currents marked by the green crosses as limiting currents, and plot these as a function of ($\sqrt{\omega}$), the obtained graph (see the green curve in Fig. 5B) will not be linear and any attempt at calculating transport parameters based on a linear fit will ultimately be erroneous. For valid analysis, we thus need to make use of an alternative method that is based on the Koutecký–Levich equation.

The Koutecký–Levich equation basically states that the current measurable under "mixed control" conditions on an RDE is the harmonic sum of the transport controlled (limiting) and the catalytic (kinetic) currents. That is,

$$I^{-1} = I_\ell^{-1} + I_{cat}^{-1}. \tag{4}$$

A rigorous mathematical derivation of the Koutecký–Levich equation will be given in the section "Theory"; for a mere qualitative understanding it is enough to make Fig. 5A subject to closer inspection. It is apparent here that the higher rotation rates we apply, the closer the obtained polarization curves will lie to the (theoretical) "catalytic current." In fact, we can reason that by applying an infinitely large rotation rate, in lieu of any transport limitation, the measured current should coincide completely with the catalytic current given in Eq. (3).

Naturally, infinite rotation rates are not practically applicable; nonetheless we can use extrapolation. To do so, in accordance with the Koutecký–Levich equation, we plot the reciprocals of currents measured at the same potential but at different rotation rates (green crosses in Fig. 5A) as a function of $\omega^{-1/2}$. As a result we obtain the straight green line shown in Fig. 5C. The intercept of this straight line (i.e., the inverse current corresponding to infinite rotation rates) gives the reciprocal catalytic current I_{cat}^{-1}, analyzing the potential dependence of which may shed light on the mechanism of the electrode reaction. The slope of the straight line, on the other hand, equals the "inverse Levich slope" $(0.620nFAD^{2/3}\nu^{-1/6}c_\infty)^{-1}$ and contains bulk transport properties such as the diffusion coefficient.

As we see, analysis based on the Koutecký–Levich equation tells more about the system under study than the Levich equation alone, since it also enables the determination of kinetic parameters. If we apply the Koutecký–Levich analysis to currents that are fully transport-limited (red dots and line in Fig. 5A), we still get a straight line with the same "inverse Levich slope" as before, but with an intercept of zero (Fig. 5C). From our previous reasoning it follows that at these potentials $I_{cat}^{-1} \approx 0$ and thus, the catalytic current (at least in comparison to the mass transfer limitations present in the system) can be considered practically infinite—yet the slope still allows us to determine parameters related to transport, just as the "simple" Levich equation would do.

I add that linearizing the Koutecký–Levich equation as in Eq. (4) is not absolutely necessary. By utilizing the fact that in case of mixed kinetics (subject to both catalytic and mass transfer limitations) the measured current is the harmonic sum of the catalytic

and transport-related currents, stationary polarization curves measured at different rotation rates can directly be made subject to nonlinear parameter estimation. In order to do so, one has to construct a model based on which an equation for the catalytic current (such as the one in Eq. 3) can be derived. For example, for the polarization curves of Fig. 5A one could assume that current (at a given overpotential $\eta = E - E_0$ and angular frequency ω) is defined as

$$I(\eta, \omega) = \frac{nFAc_\infty}{\frac{1}{k\exp\left(-\frac{\alpha n F\eta}{RT}\right)} + \frac{1}{0.620D^{2/3}\nu^{-1/6}\omega^{1/2}}}. \quad (5)$$

While some parameters of Eq. (5) (n, A, c_∞, T, ν) are usually known to the experimenter, other parameters (usually k, α, and D) can be varied and optimized to fit the polarization curves. For correct parameter optimization it is not strictly required that the polarization curves attain well-defined limiting current plateaus; reaching these, however, helps a lot in minimizing the error of optimization and the correlation of parameters.

Note that while the Levich equation (Eq. 1) only holds for limiting currents (that have essentially no potential dependence), analyses utilizing the Koutecký–Levich equation always necessitate a well-defined potential scale. That is, for the determination of kinetic parameters one needs to read currents at exactly defined electrode potential values. Consequently, *IR* drop effects must either be compensated or corrected for postexperimentally, or measures should be taken that no considerable *IR* drop occurs in the system. The latter can be achieved by using well-conducting electrolytes and by minimizing the distance (without disturbing the flow profile!) of the Luggin capillary and the working electrode surface.

As can be seen above, the analysis of RDE measurements can be expedient in determining important parameters both of electrode reactions and of transport in the bulk. A few examples to such analyses can be found among the Refs. [32,33].

Measurements With RRDEs

As it was already pointed out before (cf. Fig. 4), reversal techniques are not available with RDEs, since the product of the electrode reaction is continuously swept away from the surface of the disk.[4] Information equivalent to that available from reversal techniques at a stationary electrode can be obtained by the addition of a second electrode, as was shown in Fig. 1. The thus formed RRDE (first described by Frumkin in 1959[34]) has become one of the most convenient and widely used tools of determining electrode reaction pathways.[7]

As a typical example of so-called generator–collector assemblies, RRDEs are often used for the detection of products and intermediates formed in electrode reactions. Products formed at the disk (generator) electrode leave the disk surface and due to forced convection make their way toward the ring electrode (collector). The potential of the ring, E_{ring}, can be regulated independently from the potential of the disk, E_{disk}; that is, when an appropriate value of E_{ring} is used, the portion of disk reaction products reaching the ring electrode can undergo another electrode reaction and can thus be detected.

In an RRDE, the current–potential characteristics of the disk are unaffected by the presence of the ring and the properties of the disk are as described in the section "**Measurements With RDEs**." In fact, if the disk current is found to change upon variation of the ring potential or current, one should suspect either a defective RRDE (direct leakage between the disk and ring electrodes) or an undesirable electrical cross-talk[35–37] due to the coupling of the ring and disk through the uncompensated solution resistance. Effects related to electrical cross-talk are going to be discussed later in the section "**Digital Simulation of the RRDE System**" where it will be shown that the appearance and intensity of these effects depend heavily on the placement of the reference electrode (i.e., the tip of the Luggin capillary) within the cell.

Since RRDE experiments involve the examination of two potentials (E_{disk} and E_{ring}) and two currents (I_{disk} and I_{ring}), the representation of the results involves more dimensions than for experiments involving a single working electrode.[4] RRDE experiments thus rely on more complex instrumentation than RDE studies and require the use of a bi-potentiostat.

The first bi-potentiostat (actually, for RRDE measurements) was developed by Napp et al. in 1967. In the past few decades, several improvements have been made to these devices, which resulted in a higher bandwidth, stability of response, and convenience. A simplified circuit of a modern bi-potentiostat (PINE AFRDE5[38]) is shown in Fig. 6. The circuitry of the potentiostatic control of the disk electrode consists of the potential follower PF1 and the control amplifier CA1 (the output of which is connected to the counter electrode), and the current-to-voltage converter CTV. Serving as a current sink, CTV keeps the disk electrode at virtual ground by means of its current feedback loop; meanwhile, the amplifier CA1 maintains the difference between the disk and the reference electrode at the desired value. The circuitry required for the potentiostatic control of the second electrode (the ring) consists of the potential follower PF1, the inverter I, the control amplifier CA2, and the potential follower PF2. The role of CA2 is to make the potential difference between the ring electrode and the reference electrode equal to the voltage of the excitation signal.

As it can be seen in Fig. 6, the counter electrode is included in the control loops of both working electrodes; the current that flows through it is thus the algebraic sum of the disk and ring currents. By the application of a circuit like this, simultaneous potential control of the two working electrodes can be achieved. In many cases, however, an equally efficient bi-potentiostatic control can also be achieved by using two "single" potentiostats instead of a bi-potentiostat. The technical feasibility of this approach depends on the grounding concepts of the devices; that is, two or more potentiostats can be used in a multipontetiostat assembly provided that their circuits ground the counter (or, alternatively, the reference) and not the working electrode. For example, the XPot potentiostats manufactured by Zahner Messsysteme, Kronach, Germany[39] can be operated by placing the counter electrode to ground; thus these devices can be used to create a bi-potentiostatic setup.

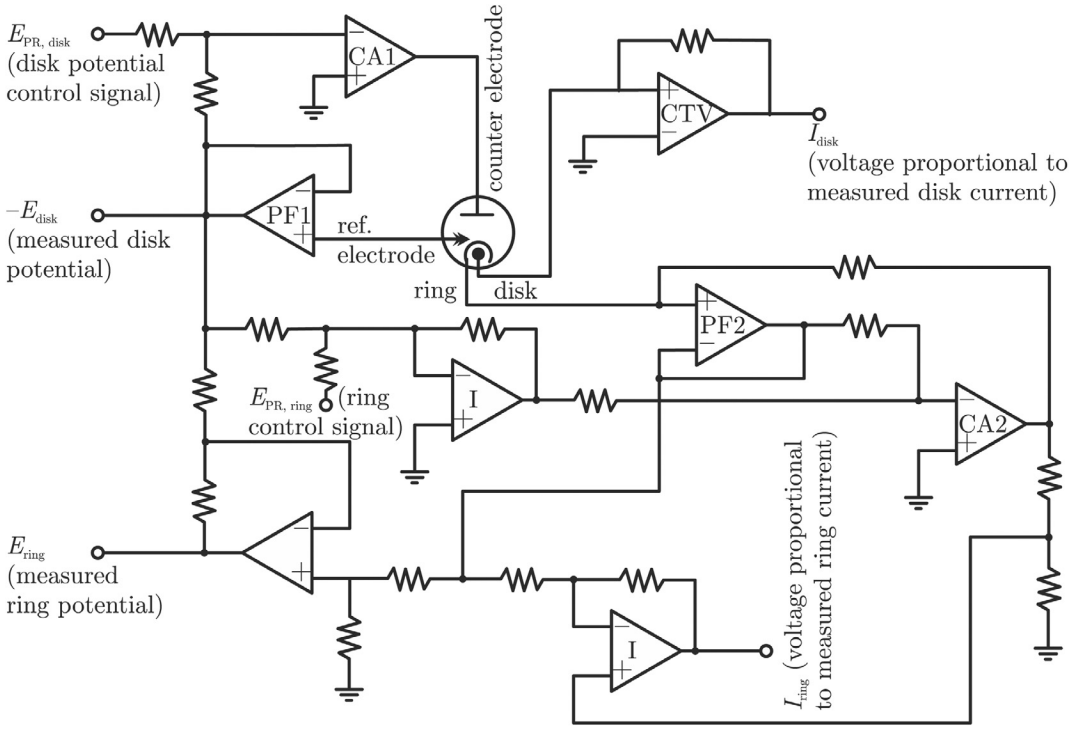

Fig. 6 Circuit schematics of a bi-potentiostat coupled to an electrochemical cell holding an RRDE, a counter, and a reference electrode.

The ability of controlling two electrode potentials independently creates a myriad of possibilities for using RRDEs; the usual approach is however to keep either one (or both) of the electrodes at constant potential or current.

For example, when using an RRDE one can record a current–potential curve (e.g., a CV) on the disk electrode, while keeping the ring at a constant potential and observing changes of the ring current. This can lead to the detection of disk-originated products, such as in case of the surface oxidation/reduction of gold electrodes,[40–42] where by keeping the ring electrode at suitably low potentials, the formation of a reducible intermediate (an oxidized gold species) can be detected (see **Fig. 7**).

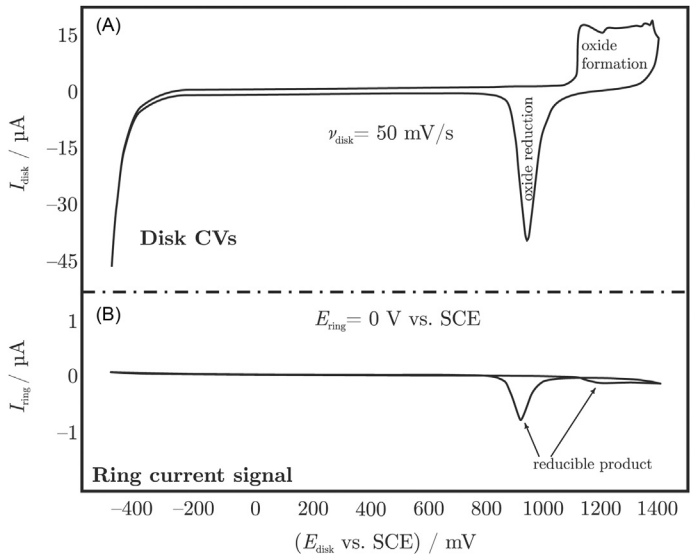

Fig. 7 (A) Cyclic voltammograms measured on the disk electrode of a gold disk–gold ring RRDE, immersed into a 0.5 mol dm^{-3} H_2SO_4 solution. CV vertices: 1400 and −500 mV versus SCE, sweep rate: 50 mV s^{-1}. (B) The ring current recorded in parallel with measuring the CVs of the disk, plotted as a function of the disk potential, reveals the formation of reducible intermediates accompanying both the oxidation and the subsequent reduction of the gold surface. Rotation rate: 500 min^{-1}, ring potential: 0 V versus SCE.

Alternatively, one may also choose to hold E_{disk} (or I_{disk}) at a constant value, and scan the ring potential: this allows the identification (and detection) of multiple products. Such experiments were carried out, for example, by Kamar and Miller[43] to study the corrosion of La_2CuO_4 in aqueous media.

In the above-mentioned "collection" experiments, the aim is to bring a disk-generated product into reaction at the ring surface. It is important to note, however, that only a certain ratio of disk-generated products can get close to the ring electrode: some amount necessarily diffuses away toward the bulk solution and escapes detection. In order to express this behavior, one can define a"collection efficiency" for RRDE systems.

In practice, the collection efficiency $\mathcal{N}$ is measured under well-defined conditions. For example, in a system that contains a reducible species, one can set a disk potential that is negative enough so that at a certain rotation rate a cathodic (limiting) current can be measured. In the meantime, the ring potential can be set to positive values so that any reduced product formed on the disk, when reaching the ring electrode, would immediately be oxidized back. The collection efficiency can then be defined as

$$\mathcal{N} = \frac{I_{ring} n_{disk}}{I_{disk} n_{ring}}, \tag{6}$$

where n_{disk} and n_{ring} denote the number of electrons transferred in the disk and ring electrode reactions. (Note that in most cases, $n_{ring} = -n_{disk}$.) By definition, $\mathcal{N}$ is a positive number less than unity; usual values range between 25% and 37%.

In measurements we usually find that at high enough rotation rates, the collection efficiency $\mathcal{N}$ does not depend on the applied rotation rate and is only a function of the geometric parameters of the RRDE. A theoretical expression for $\mathcal{N}$ was derived in 1966 by Albery and Bruckenstein[8]:

$$\mathcal{N} = 1 - F(\alpha/\beta) + \beta^{2/3}(1 - F(\alpha)) - (1 + \alpha + \beta)^{2/3}\left(1 - F\left(\frac{\alpha + \alpha^2 + \alpha\beta}{\beta}\right)\right), \tag{7}$$

where

$$\alpha = \left(\frac{r_2}{r_1}\right)^3 - 1, \tag{8}$$

$$\beta = \frac{r_3^3}{r_1^3} - \frac{r_2^3}{r_1^3}, \tag{9}$$

and the function $F(\theta)$ is defined as

$$F(\theta) = \frac{\sqrt{3}}{4\pi}\ln\left(\frac{\left(1 + \sqrt[3]{\theta}\right)^3}{1 + \theta}\right) + \frac{3}{2\pi}\arctan\left(\frac{2\sqrt[3]{\theta} - 1}{\sqrt{3}}\right) + \frac{1}{4}. \tag{10}$$

(For the dimensions r_1, r_2, and r_3, see **Fig. 1**.)

RRDE experiments are not always conducted in a collection mode: sometimes, RRDEs are also used to study shielding. In shielding experiments, the ring is set to a potential value where bulk species react on its surface yielding a current I_{ring_0} when the disk is not polarized. Then, by setting the disk electrode also to a potential where the same reaction occurs, this will reduce the current measurable on the ring electrode (as a portion of the reactants which could otherwise reach the ring would now react on the disk). In this case the measurable ring current is

$$I_{ring} = I_{ring_0} - \mathcal{N} I_{disk}. \tag{11}$$

Although most of the standard RRDE techniques involve static control (at least at one of the electrodes), and thus these techniques focus on the study of either collection or of shielding effects, recent advances in the instrumentation of RRDE systems also enable the simultaneous study of both effects.[44] This necessitates the application of potentiodynamic control of both the disk and the ring electrode at the same time. For example, by a slow scanning of the disk potential and a synchronous high-rate cycling of the ring, shielding and collection effects accompanying oxygen reduction on gold were analyzed[45] (see **Fig. 8**).

Theory

As I pointed out before, RDEs (and RRDEs) owe their popularity to the fact that measurements involving them can be modeled relatively simply.

When modeling electrode processes, our aim is usually to derive mathematical expressions that can predict measured results; for example, for RDEs, stationary polarization curves like those shown in **Fig. 5**A. To do so, we have to consider and describe in a mathematical form the electrode reaction. Then we need to consider the effect of mass transfer in the solution phase that resupplies reactants to the electrode reaction and also takes products away. Transport, by nature, is a space-dependent process, while the electrode reaction is confined to a certain plane (the electrode surface). Thus what we usually do when modeling electrode processes is that we aim to solve the equations of transport under certain boundary conditions that are determined by the electrode reaction. This can

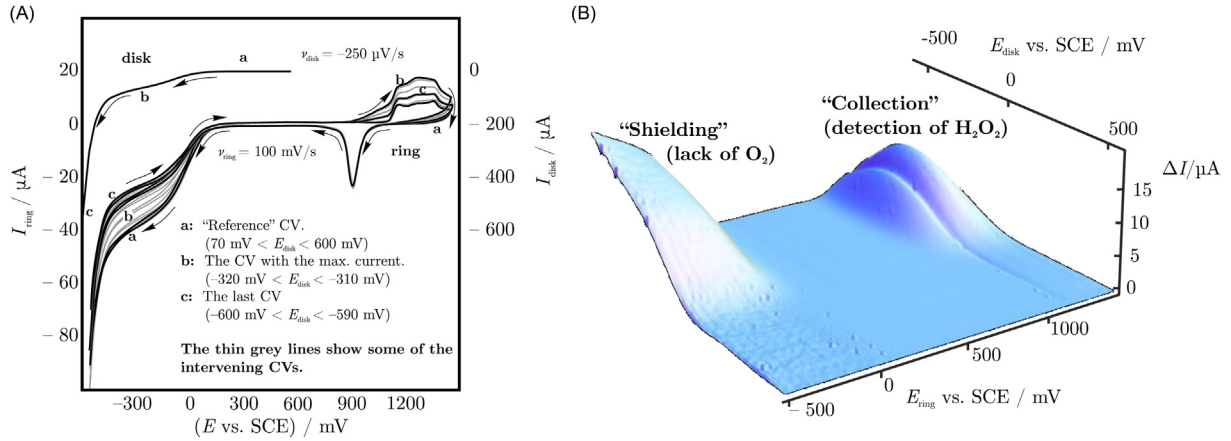

Fig. 8 (A) The shape of the CVs measured on the ring change when oxygen reduction occurs on the disk electrode of an Au–Au RRDE in an air-saturated 0.5 mol dm^{-3} sulfuric acid solution. The polarization curve obtained from the disk and a few ring CVs are shown together. (B) Changes of the ring CVs (*vs.* the "reference CV" shown in (A)), visualized as a function of the disk and ring potentials. The "3D map" of the oxygen reduction process reveals both the shielding of the ring that arises from the reduction of oxygen at the disk, and also an anodic peak that is caused by the oxidation of the hydrogen-peroxide formed at the disk. For details of the experiment, see Ref. [45].

result in the determination of (either stationary or time-dependent) concentration profiles for the species involved in the electrode process. Knowing the profiles, determining currents is just one step ahead.

The physical laws describing mass transfer dictate that the $\boldsymbol{J}_i$ flux of a species i (i.e., the amount of substance dn_i that passes a certain, arbitrarily chosen area A within an infinitesimal time-step dt) is determined as

$$\boldsymbol{J}_i = \frac{1}{A}\frac{dn}{dt} = -D_i \,\mathrm{grad}\, c_i + c_i\boldsymbol{v} + \frac{z_i F D_i c_i}{RT}\mathrm{grad}\phi + \text{other terms}. \tag{12}$$

That is, flux is determined by the rate of diffusion, convection, and migration, as described by the three terms in Eq. (12); in some cases other terms (e.g., describing homogeneous reactions in the bulk) can also be added. In what follows we will only focus on problems where homogeneous reactions do not occur and the effect of migration (i.e., the movement of a species carrying z_i charge in response to an electrical field ϕ) is also neglected. Thus, our considerations will only apply to systems that contain a supporting electrolyte in large concentration, shielding the electric potential so that grad $\phi = 0$. This leaves us with only two terms present on the right-hand side of Eq. (12). Eq. (12) now tells us that when a certain amount of substance moves through a given surface area A in the system, then this movement is either due to flow (of velocity $\boldsymbol{v}$) or due to diffusion. Note that in the absence of convection ($\boldsymbol{v} = 0$), Eq. (12) reduces to Fick's first law of diffusion.

Let us assume now that the area A we choose to write Eq. (12) for (this can be chosen arbitrarily) is that surrounding a closed volume V. We can now argue—since chemical reactions are not taking place—that any change of the amount of substance within this volume V can only occur if some amount of substance leaves or enters the bounding area A. That is, by integrating concentration changes inside the volume V over V, we must get the same result as if we would integrate the flux over the area A, or (by using the Gauss–Ostrogradsky theorem) if we would integrate the divergence of the flux over V. That is,

$$\int_V \frac{\partial c_i}{\partial t} dV = \oint_A -\boldsymbol{J}_i dA = \int_V -\,\mathrm{div}\,\boldsymbol{J}_i dV. \tag{13}$$

From this and from the remaining terms in Eq. (12) it follows that

$$\frac{\partial c_i}{\partial t} = \mathrm{div}\,(D_i \,\mathrm{grad}\, c_i) - \mathrm{div}\,(c_i\boldsymbol{v}), \tag{14}$$

or, if we assume that the diffusion coefficient D_i is a constant independent of space and the fluid is incompressible so that div $\boldsymbol{v} = 0$,

$$\frac{\partial c_i}{\partial t} = D_i \,\mathrm{div}\,\mathrm{grad}\, c_i - \boldsymbol{v}\cdot\mathrm{grad}\, c_i. \tag{15}$$

When dealing with hydrodynamical techniques, the convective–diffusion equation we usually aim to solve is Eq. (15). The solution then yields concentration profiles based on which the flux of the different species at the electrode surface can be calculated (using Eq. 12) and finally, the current can be determined.

In order to find a solution for Eq. (15), expressions for the velocity profile $\boldsymbol{v}$ must be obtained. Generally, $\boldsymbol{v} = \boldsymbol{v}(\boldsymbol{x}, t)$ is a vector field that depends both on time and spatial coordinates; however in many cases (such as for the majority of rotating electrode techniques) we assume that the flow is stationary.

Fluid Flow Under a Rotating Disk

In an incompressible fluid, flow profiles are described by the Navier–Stokes equation

$$\frac{d\boldsymbol{v}}{dt} = -\text{grad}\frac{p}{\varrho} + \nu\,\text{div grad}\,\boldsymbol{v} + \frac{f}{\varrho} \tag{16a}$$

and the equation of continuity,

$$\text{div}\,\boldsymbol{v} = 0. \tag{16b}$$

The simple form of the Navier–Stokes equation given in Eq. (16a) is in fact a formulation of Newton's first law for a given solution volume. It states that any acceleration of the fluid $\left(d\boldsymbol{v}/dt\right)$ arises from the negative gradient of pressure over density $\left(\text{grad}-p/\varrho\right)$ as well as from any outer force f applied to the fluid (normalized with the density ϱ). Velocity losses arise as a result of dissipation of the kinetic energy due to internal friction, as represented by the term ν div grad $\boldsymbol{v}$, where ν is the kinematic viscosity of the liquid.

The theoretical treatment of RDEs requires the solution of the Navier–Stokes equation for a system that consists of an infinitely large disk rotating in a viscous medium. This problem was first studied and solved by the Hungarian scientist Tódor Kármán in 1921,[46] followed by a more accurate solution of Cochran in 1934.[47] The results of Kármán and Cochran were used by Levich when formulating the theory of RDEs.[5]

The symmetry of the rotating disk system suggests that the problem should be treated using cylindrical coordinates, as shown in Fig. 9. In order to describe the flow profile, we place a disk of infinite radius (i.e., a suitably large disk) centered on the origin of the coordinate system, with its axis of rotation aligned to the z-axis. (A practical consequence of the assumptions taken for solving the Navier–Stokes equations is that the rotated mantle should be appropriately thick: usually, the dimension $r_0 > 0.5$ cm (see Fig. 1).)

If we write out the differential operators in Eqs. (16a) and (16b) using cylindrical coordinates, we obtain the following system of partial differential equations that describe the v_r, v_φ, and v_z velocity components:

$$\overbrace{\frac{\partial v_r}{\partial t}}^{0^{(i)}} + v_r\frac{\partial v_r}{\partial r} + \overbrace{\frac{v_\varphi}{r}\frac{\partial v_r}{\partial \varphi}}^{0^{(ii)}} + v_z\frac{\partial v_r}{\partial z} - \frac{v_\varphi^2}{r} = \underbrace{-\frac{\partial}{\partial r}\left(\frac{p}{\varrho}\right)}_{0^{(iii)}} + \nu\left[\frac{1}{r}\frac{\partial}{\partial r}\left(r\frac{\partial v_r}{\partial r}\right) + \underbrace{\frac{1}{r^2}\frac{\partial^2 v_r}{\partial \varphi^2}}_{0^{(iii)}} + \frac{\partial^2 v_r}{\partial z^2} - \frac{v_r}{r^2} - \underbrace{\frac{2}{r^2}\frac{\partial v_\varphi}{\partial \varphi}}_{0^{(iii)}}\right] + \underbrace{f_r}_{0^{(iv)}} \tag{17a}$$

$$\overbrace{\frac{\partial v_\varphi}{\partial t}}^{0^{(i)}} + v_r\frac{\partial v_\varphi}{\partial r} + \overbrace{\frac{v_\varphi}{r}\frac{\partial v_\varphi}{\partial \varphi}}^{0^{(ii)}} + v_z\frac{\partial v_\varphi}{\partial z} - \frac{v_r v_\varphi}{r} = \underbrace{-\frac{1}{r}\frac{\partial}{\partial \varphi}\left(\frac{p}{\varrho}\right)}_{0^{(iii)}} + \nu\left[\frac{1}{r}\frac{\partial}{\partial r}\left(r\frac{\partial v_\varphi}{\partial r}\right) + \underbrace{\frac{1}{r^2}\frac{\partial^2 v_\varphi}{\partial \varphi^2}}_{0^{(iii)}} + \frac{\partial^2 v_\varphi}{\partial z^2} - \frac{v_\varphi}{r^2} - \underbrace{\frac{2}{r^2}\frac{\partial v_r}{\partial \varphi}}_{0^{(iii)}}\right] + \underbrace{f_\varphi}_{0^{(iv)}} \tag{17b}$$

$$\overbrace{\frac{\partial v_z}{\partial t}}^{0^{(i)}} + \overbrace{v_r\frac{\partial v_z}{\partial r}}^{0^{(v)}} + \overbrace{\frac{v_\varphi}{r}\frac{\partial v_z}{\partial \varphi}}^{0^{(ii)}} + v_z\frac{\partial v_z}{\partial z} = -\frac{\partial}{\partial z}\left(\frac{p}{\varrho}\right) + \nu\left[\underbrace{\frac{1}{r}\frac{\partial}{\partial r}\left(r\frac{\partial v_z}{\partial r}\right)}_{0^{(v)}} + \underbrace{\frac{1}{r^2}\frac{\partial^2 v_z}{\partial \varphi^2}}_{0^{(iii)}} + \frac{\partial^2 v_z}{\partial z^2}\right] + \underbrace{f_z}_{0^{(iv)}} \tag{17c}$$

$$0 = \frac{1}{r}\frac{\partial}{\partial r}(rv_r) + \underbrace{\frac{1}{r}\frac{\partial v_\varphi}{\partial \varphi}}_{0^{(iii)}} + \frac{\partial v_z}{\partial z} \tag{17d}$$

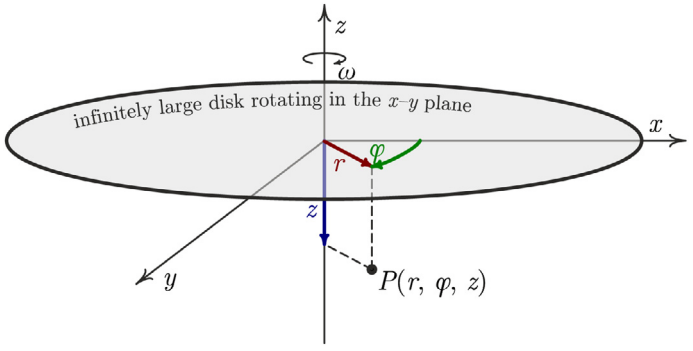

Fig. 9 A system of cylindrical coordinates showing a point P of coordinates r, φ, and z. The disk is placed in the x y plane, rotating around the point at $r = 0$ with constant angular velocity ω.

Inspection of Eqs. (17a)–(17d) reveals that several terms cancel out because of either one of the following reasons:

(i) All temporal derivatives are considered zero: this will lead to a solution for the stationary flow profile.
(ii) All derivatives with respect to the angular coordinate φ vanish due to the axial symmetry of the system.
(iii) Due to the horizontal alignment of the disk, the derivative of pressure p with respect to the radial coordinate r vanishes.
(iv) External forces (such as due to gravity) are considered negligible so that all entries of the vector f are treated as zero.
(v) Since the disk is considered infinitely large, the axial velocity component is independent of the radial coordinate and thus $\partial v_z/\partial r = 0$.

The above considerations, when used to simplify Eqs. (17a)–(17d), result in the following system of partial differential equations describing stationary flow:

$$v_r\frac{\partial v_r}{\partial r} + v_z\frac{\partial v_r}{\partial z} - \frac{v_\varphi^2}{r} = \nu\left[\frac{1}{r}\frac{\partial}{\partial r}\left(r\frac{\partial v_r}{\partial r}\right) + \frac{\partial^2 v_r}{\partial z^2} - \frac{v_r}{r^2}\right] \tag{18a}$$

$$v_r\frac{\partial v_\varphi}{\partial r} + v_z\frac{\partial v_\varphi}{\partial z} - \frac{v_r v_\varphi}{r} = \nu\left[\frac{1}{r}\frac{\partial}{\partial r}\left(r\frac{\partial v_\varphi}{\partial r}\right) + \frac{\partial^2 v_\varphi}{\partial z^2} - \frac{v_\varphi}{r^2}\right] \tag{18b}$$

$$v_z\frac{\partial v_z}{\partial z} = -\frac{\partial}{\partial z}\left(\frac{p}{\varrho}\right) + \nu\frac{\partial^2 v_z}{\partial z^2} \tag{18c}$$

$$0 = \frac{1}{r}\frac{\partial}{\partial r}(r v_r) + \frac{\partial v_z}{\partial z} \tag{18d}$$

To solve Eqs. (18a)–(18d), we formulate two boundary conditions. One of these is a so-called no-slip condition at the surface of the disk; that is, the fluid layer adjacent to the rotating disk surface moves together with it, and thus

$$v_r = 0, \quad v_\varphi = \omega r \quad \text{and} \quad v_z = 0 \quad \text{at} \quad z = 0. \tag{19}$$

That the rotating disk drags the nearby fluid layer (which then moves together with the disk) implies that there is a significant radial velocity at not very high distances below the rotating surface, in the direction outward from the axis of rotation. Due to the requirement of continuity, this radial outflow must be compensated by an axial inflow that should—since the disk is infinitely or, at least in practice, very large—not depend on the radial coordinate. This results in the following boundary condition:

$$v_r = 0, \quad v_\varphi = 0 \quad \text{and} \quad v_z = -v_\infty \quad \text{at} \quad z = \infty. \tag{20}$$

By introducing at this point the dimensionless variable

$$\zeta = z\sqrt{\frac{\omega}{\nu}} \tag{21}$$

and the scaling functions $F(\zeta)$, $G(\zeta)$, $H(\zeta)$, and $P(\zeta)$ so that

$$v_r = r\omega F(\zeta), \tag{22a}$$

$$v_\varphi = r\omega G(\zeta), \tag{22b}$$

$$v_z = \sqrt{\nu\omega}H(\zeta), \tag{22c}$$

$$p = -\varrho\nu\omega P(\zeta), \tag{22d}$$

the system of partial differential Eqs. (18a)–(18d) can be cast into the following system of ordinary differential equations:

$$F^2 + F'H = F'' + G^2 \tag{23a}$$

$$2FG + G'H = G'' \tag{23b}$$

$$2F + H' = 0 \tag{23c}$$

$$HH' = P' + H''. \tag{23d}$$

Note that the scaling function for pressure, $P(\zeta)$, appears only in Eq. (23d) and thus this equation can be decoupled from the system of ordinary differential equations (23a)–(23c) describing the flow velocity components. Unfortunately, no exact solution was found so far for this system of equations. In 1934, Cochran provided an approximate solution in the form of finite-term series and by optimizing the coefficients.[47] More than 80 years later it seems simpler (and more accurate) to look for a numerical solution.

A numerical solution to Eqs. (23a)–(23c) can be found by assuming we know what initial values (at $\zeta = 0$) the functions F, G, and H as well as the derivatives F' and G' take. Then $H'(0)$ can already be found from Eq. (23c) and values of the second derivatives

$F''(0)$ and $G''(0)$ can also be expressed from Eqs. (23a) and (23b), respectively. Knowing these initial values we could then start an iteration, increasing in each step the independent variable ζ by small steps of $\triangle\ \zeta$ and determining in each kth step new function and derivative values, based on values defined in the previous step $(k-1)$. That is,

$$F_k = F_{k-1} + \Delta\zeta F'_{k-1} \tag{24a}$$

$$G_k = G_{k-1} + \Delta\zeta G'_{k-1} \tag{24b}$$

$$H_k = H_{k-1} + \Delta\zeta H'_{k-1} \tag{24c}$$

$$F'_k = F'_{k-1} + \Delta\zeta F''_{k-1} \tag{24d}$$

$$G'_k = G'_{k-1} + \Delta\zeta G''_{k-1} \tag{24e}$$

and then,

$$H'_k = -2F_k \tag{24f}$$

$$F''_k = F_k^2 + F'_k H_k - G_k^2 \tag{24g}$$

$$G''_k = 2F_k G_k - G'_k H_k. \tag{24h}$$

This iteration, started from $\zeta = 0$, can be used to generate numerical values at fine $\Delta\zeta$ steps for the functions F, G, and H. All it requires is the knowledge of the $F(0)$, $G(0)$, $H(0)$, $F'(0)$, and $G'(0)$ initial values.

The only problem of the above method is that some of the initial values are not known. The boundary conditions given by Eqs. (19) and (20), when written for the dimensionless scaling functions, translate to

$$F(0) = 0, \quad G(0) = 1; \quad H(0) = 0, \quad \lim_{\zeta\to\infty} F(\zeta) = 0 \quad \text{and} \quad \lim_{\zeta\to\infty} F(\zeta) = 0. \tag{25}$$

That is, instead of having initial values for the derivatives F' and G', we have final values (as $\zeta \to \infty$) for the functions F and G. In order to still find a numerical solution for Eqs. (23a)–(23c), we thus utilize the so-called shooting method. This requires that we make an initial guess for the values of $F'(0)$ and $G'(0)$ and then do an iterative solution which goes to large values of ζ. The obtained F and G functions will probably not reach 0 (as they should) when ζ tends to infinity; however in subsequent iterations we can modify the initial guess and improve the asymptotic behavior.

The shooting method results in reliable solutions for the functions F, G, and H that are tabulated as a function of ζ in Table 1. Based on Eqs. (22a)–(22c), the velocity profile components v_r, v_φ, and v_z can be calculated using the function values listed in Table 1 for given values of ν and ω.

Fluid motion due to convective flow is illustrated by Fig. 10A: here a chosen fluid volume first approaches (mostly by movement in the z direction), then leaves (by radial out-drift) a disk electrode rotated as part of a larger plane.

The functions $F(\zeta)$, $G(\zeta)$, and $H(\zeta)$ are plotted versus ζ in Fig. 10B. Here the series approximations of Cochran,[47] valid for $\zeta \ll 1$, are also shown (see the dashed lines in Fig. 10B):

$$F(\zeta) = a\zeta - \frac{\zeta^2}{2} - \frac{b\zeta^3}{3} + \cdots \tag{26a}$$

$$G(\zeta) = 1 + b\zeta + \frac{a\zeta^3}{3} + \cdots \tag{26b}$$

$$H(\zeta) = -a\zeta^2 + \frac{\zeta^3}{3} + \frac{b\zeta^4}{6} + \cdots \tag{26c}$$

The coefficients in Eqs. (26a)–(26c) were determined by Cochran[47] as $a = 0.51023$ and $b = -0.6159$.

Stationary Concentration Profiles and Currents at RDEs

Once the velocity profile has been determined, the convective–diffusion equation, Eq. (15), can be solved for the RDE. First we point out that RDEs (provided that not only the rotating shaft but also the electrode has a large enough radius) can in almost all cases be safely treated as one-dimensional systems. That is, the current of a large enough RDE will not be affected by radial transport, and thus Eq. (15)—assuming only one transferred species—simplifies to

$$\frac{\partial c}{\partial t} = D\frac{\mathrm{d}^2 c}{\mathrm{d}z^2} - v_z\frac{\mathrm{d}c}{\mathrm{d}z}, \tag{27}$$

Table 1 The scaling functions $F(\zeta)$, $G(\zeta)$, and $-H(\zeta)$ evaluated at different values of the dimensionless variable ζ

ζ	$F(\zeta)$	$G(\zeta)$	$-H(\zeta)$
0	0.000000	1.000000	0.000000
0.001	0.000510	0.999384	0.000001
0.002	0.001018	0.998768	0.000002
0.005	0.002539	0.996920	0.000013
0.01	0.005053	0.993841	0.000051
0.02	0.010006	0.987683	0.000201
0.03	0.014862	0.981527	0.000450
0.04	0.019622	0.975374	0.000795
0.05	0.024287	0.969224	0.001235
0.06	0.028858	0.963080	0.001766
0.07	0.033336	0.956941	0.002388
0.08	0.037722	0.950809	0.003099
0.09	0.042018	0.944684	0.003897
0.1	0.046225	0.938567	0.004779
0.2	0.083636	0.878013	0.017903
0.3	0.113341	0.819020	0.037720
0.4	0.136359	0.762091	0.062793
0.5	0.153623	0.707580	0.091880
0.6	0.165974	0.655724	0.123915
0.7	0.174168	0.606664	0.157993
0.8	0.178879	0.560464	0.193351
0.9	0.180700	0.517132	0.229352
1.0	0.180156	0.476627	0.265473
1.1	0.177701	0.438876	0.301287
1.2	0.173729	0.403779	0.336452
1.3	0.168581	0.371223	0.370700
1.4	0.162543	0.341078	0.403826
1.5	0.155862	0.313213	0.435675
1.6	0.148741	0.287490	0.466141
1.7	0.141352	0.263774	0.495153
1.8	0.133835	0.241931	0.522673
1.9	0.126304	0.221831	0.548687
2	0.118851	0.203349	0.573200
3	0.058120	0.084523	0.745244
4	0.025668	0.034945	0.825059
5	0.010893	0.014433	0.859605
10	0.000133	0.000173	0.884173
20	0.000000	0.000000	0.884474
∞	0.000000	0.000000	0.884474

which is a differential equation for one dimension (containing only the z spatial coordinate). Let us now focus on the determination of the stationary profile (for which $\partial c/\partial t = 0$) and express v_z using Eq. (22c) and the first-term approximation of Eq. (26c). By this we arrive to the following ordinary differential equation determining the stationary concentration profile:

$$0 = D\frac{\mathrm{d}^2 c}{\mathrm{d}z^2} + az^2\sqrt{\frac{\omega^3}{\nu}}\,\frac{\mathrm{d}c}{\mathrm{d}z}. \tag{28}$$

The general solution of this differential equation is a function of the form

$$c(z) = \chi_2 - \frac{1}{3}z\chi_1 E_{2/3}\left(\frac{az^3}{3D_i}\sqrt{\frac{\omega^3}{\nu}}\right). \tag{29}$$

The function $E_p(x)$, appearing in Eq. (29), is called the generalized exponential integral function and it is defined by the integral $E_p(x) = \int_1^\infty u^{-p}\exp(-xu)\mathrm{d}u$. The generalized exponential integral function is related by the formula $E_p(x) = x^{(p-1)}\Gamma(1-p,x)$ to the (upper) incomplete gamma function $\Gamma(s, x)$, defined as $\Gamma(s,x) = \int_x^\infty u^{s-1}\exp(-u)\mathrm{d}u$. In Eq. (29), χ_1 and χ_2 are integration constants defined as

$$\chi_2 = \lim_{z\to\infty} c(z) = c_\infty \tag{30}$$

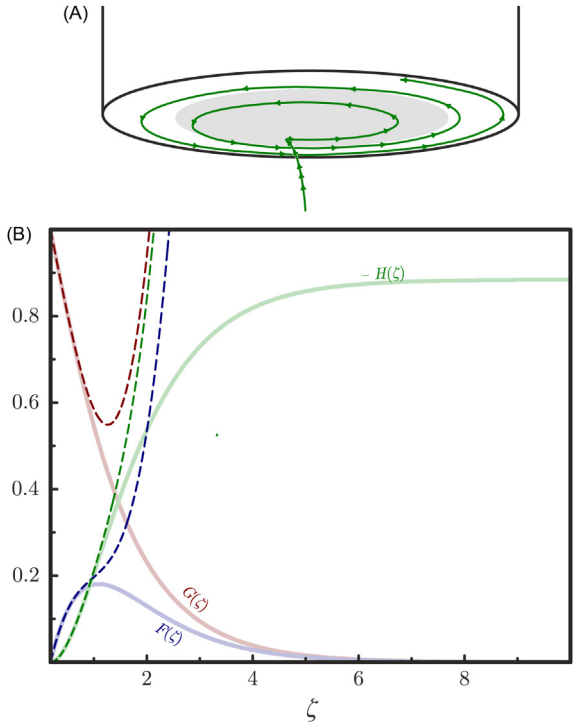

Fig. 10 (A) The trajectory of a chosen fluid volume that first approaches (mostly by movement in the z direction), then leaves (by radial out-drift) a disk electrode rotated as part of a larger plane. (B) The scaling functions $F(\zeta)$, $G(\zeta)$, and $-H(\zeta)$, evaluated at different values of the dimensionless variable ζ. Approximative solutions given by Eqs. **(26a)–(26c)** are shown by the dashed curves.

and

$$\chi_1 = \lim_{z\to 0^+} \frac{\mathrm{d}c(z)}{\mathrm{d}z} = c'(0). \tag{31}$$

That is, the integration constant χ_2 is in fact the bulk concentration of the reacting species c_∞ and χ_1 is the gradient of the concentration profile at the position of the electrode plane, $c'(0)$. It is also expedient to express the near-surface concentration value c_0 as

$$c_0 = \lim_{z\to 0^+} c(z) = c_\infty - \frac{D^{1/3}\nu^{1/6}c'(0)\Gamma\left(\frac{1}{3},\,0\right)}{3^{2/3}a^{1/3}\omega^{1/2}}. \tag{32}$$

From Eq. **(32)**, the integration constant $c'(0)$ can be expressed in terms of c_0 and can directly be plugged into Eq. **(29)** to yield a concentration profile parametrized by the near-surface concentration c_0 and the bulk concentration c_∞:

$$c(z) = c_\infty - (c_\infty - c_0)\frac{\Gamma\left(\frac{1}{3},\,\frac{az^3\omega^{3/2}}{3D\sqrt{\nu}}\right)}{\Gamma\left(\frac{1}{3},\,0\right)}. \tag{33}$$

Concentration profiles for two different near-surface and bulk concentration ratios ($c_0/c_\infty = 0$ and 0.5) are plotted in **Fig. 11**. Note that in **Fig. 11** the dimensionless concentration c/c_0 is plotted against the distance measured from the electrode surface, expressed here in multiples of the so-called diffusion layer thickness δ.

As shown by the dashed lines in **Fig. 11**, δ is the distance where the first-order approximations of the concentration profiles intersect with the value of c_∞. The diffusion layer thickness, as can be seen in the figure, is independent from the actual value of c_0 and of c_∞.

Mathematically, the diffusion layer thickness δ can be expressed by expanding Eq. **(33)** around $z = 0$ to the first order, equating the thus-obtained expression to $c\,\infty$ and then solving for z. This gives

$$\delta = \frac{\nu^{1/6}\Gamma\left(\frac{1}{3},\,0\right)D^{1/3}}{3^{2/3}a^{1/3}\sqrt{\omega}} \approx 1.6117\nu^{1/6}D^{1/3}\omega^{-1/2}. \tag{34}$$

Having determined the concentration profiles, expressing the stationary current measurable on RDEs is just a single step forward. At this point I refer back to Eq. **(12)**, which states that the flux of a species (through a given surface A) is determined as a sum of diffusive and convective (sometimes also migration-related and other) terms. Since the current of the RDE is in fact the flux of the reacting species scaled by nF (where n is the number of electrons transferred in the electrode reaction and F is Faraday's constant), the current of the RDE is

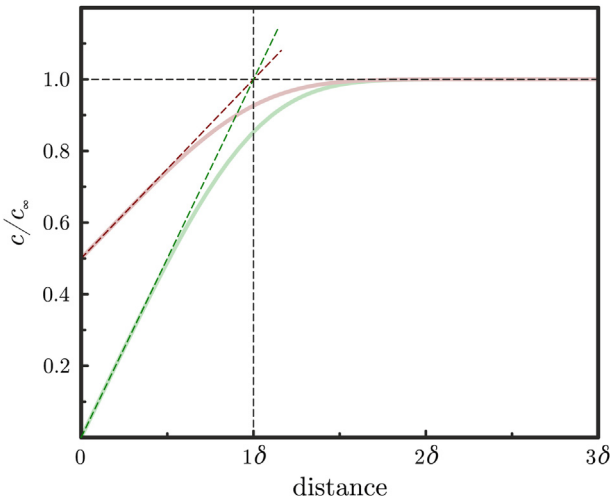

Fig. 11 Dimensionless stationary concentration profiles for an RDE, plotted as a function of dimensionless distance (distance is expressed as multiples of the diffusion layer thickness defined by Eq. (34)). For the profiles plotted by the red and the green curves, $c_0 = 0$ and $c_0 = \frac{c_\infty}{2}$, respectively. First-order series approximations are shown by the slanted dashed lines: note their intersection with the c_∞ level at 1δ.

$$I = nFADc'(0) \tag{35}$$

where, for the sake of simplicity, we now assumed that there is only one electrode reaction taking place. By expressing $c'(0)$ from Eq. (32) and substituting to Eq. (35) we arrive to

$$I = nFA(c_\infty - c_0)\frac{3^{2/3}a^{1/3}D^{2/3}\omega^{1/2}}{\nu^{1/6}\Gamma\left(\frac{1}{3}, 0\right)} = nFAD\frac{c_\infty - c_0}{\delta}. \tag{36}$$

When limiting currents are measured (i.e., when the reaction is so fast that $c_0 = 0$), Eq. (36) reduces to the Levich equation (Eq. 1) and gives

$$I_\ell = nFAc_\infty\frac{3^{2/3}a^{1/3}D^{2/3}\omega^{1/2}}{\nu^{1/6}\Gamma\left(\frac{1}{3}, 0\right)} \approx 0.620nFAD^{2/3}\nu^{-1/6}c_\infty\omega^{1/2}. \tag{37}$$

It follows from Eq. (36) and from the definition of the limiting current, Eq. (37), that for non-limiting stationary currents the equation

$$\frac{I}{I_\ell} = \frac{c_\infty - c_0}{c_\infty} \tag{38}$$

holds. Provided that the current of the charge-transfer reaction is scaled linearly with the near-surface concentration (as it is true for Eq. 2), we are always able to define a catalytic current (such as we did in Eq. 3) that scales linearly with c_∞. The measurable current I is then always smaller than the catalytic current I_{cat}, and

$$\frac{I}{I_{cat}} = \frac{c_0}{c_\infty}. \tag{39}$$

Uniting Eqs. (38) and (39) then yields the Koutecký–Levich equation, Eq. (4).

Digital Simulation of the RRDE System

As it was shown earlier, deriving closed-form expressions (like the Levich and Koutecký–Levich equations) useful for the analysis of RDE measurements was relatively simple. This is due to the fact that in most cases, RDE systems can be treated as one-dimensional problems. The same cannot be said for RRDEs; in order to describe RRDEs, it is essential to take mass transfer fully into consideration (also in the radial, not only in the axial direction).

As a result, deriving closed-form expressions for RRDEs may become overly complicated (although not necessarily impossible: e.g., Eq. (7) defining the collection efficiency of RRDEs was derived analytically[8]). Digital simulations offer, however, a possible alternative for the description of RRDE systems and nowadays several software packages are available which can make such simulations straightforward. Therefore, in what follows I shall attempt to give an introduction to the simulation of the RRDE systems. Several such simulations—of varying scope and accuracy—were devised in the past[48,49]: the approach we follow here was described in detail in Refs. [50,51].

The simulation strategy I describe here can be found useful, for example, for the analysis of electrical cross-talk effects that were described previously in the section "**Measurements With RRDEs**." Note that similar approaches can be used also for the modeling of other electrochemical systems where multiple working electrodes are used.

For the sake of simplicity, in this chapter we confine our attention to a finite-resistance solution of two electrochemically active species (denoted by Red and Ox) in which a RRDE tip is immersed. Initially, both Red and Ox have a uniform concentration distribution in the system; however at the disk and ring surfaces the two electroactive species undergo the (1-electron) electrode reaction

$$\mathrm{Ox} + \mathrm{e}^- \rightleftharpoons \mathrm{Red}. \tag{40}$$

Also for the sake of simplicity we will assume that the above reaction is reversible, and thus dictates that the concentrations of the two species in the vicinity of the two electrodes should always fulfil the following equation:

$$\frac{c_{\mathrm{Ox\ near\ disk\ or\ ring}}}{c_{\mathrm{Red\ near\ disk\ or\ ring}}} = \exp\left[\frac{\left(E_{\mathrm{disk\ or\ ring}} - E^{\ominus}\right)F}{RT}\right], \tag{41}$$

that is, the well-known Nernst equation. It should be mentioned here that taking into account irreversible reactions would also be possible within the framework of finite volume simulations by an analytical integration of the Erdey-Grúz–Volmer equation for a given control volume, as it was described, for example, in Ref. [52].

We further assume that the concentration changes occurring near the disk and ring surfaces propagate through the system under study as described by the following mass transfer equations:

$$\frac{\partial c_{\mathrm{Ox}}}{\partial t} = D_{\mathrm{Ox}}\,\mathrm{div\ grad}\ c_{\mathrm{Ox}} - \boldsymbol{v}\cdot\mathrm{grad}\ c_{\mathrm{Ox}}, \tag{42a}$$

$$\frac{\partial c_{\mathrm{Red}}}{\partial t} = D_{\mathrm{Red}}\,\mathrm{div\ grad}\ c_{\mathrm{Red}} - \boldsymbol{v}\cdot\mathrm{grad}\ c_{\mathrm{Red}}, \tag{42b}$$

where D_{Ox} and D_{Red} are the diffusion coefficients of the reacting species, and $\boldsymbol{v} = \boldsymbol{v}(r, z)$ is the velocity profile of the hydrodynamic flow.

In Eqs. **(42a) and (42b)** we assume that the mass transfer of any electroactive species takes place only by means of diffusion and convection, and that concentration changes due to any other effects (e.g., migration) are negligible. In Eqs. **(42a)** and **(42b)** we further assume that each diffusing species have a constant diffusion coefficient (D_{Ox} and D_{Red} are independent, for example, from the concentration), and that the stationary velocity profile $\boldsymbol{v}$ is that determined numerically in the section "**Fluid Flow Under a Rotating Disk**."

In simulations of RRDE systems we can consider a solution of finite electrical resistivity. We may further assume that the species Red and Ox are present in concentrations low enough (compared to that of the supporting electrolyte) so that the resistivity of the solution is undisturbed by any changes of c_{Red} and c_{Ox}, and it is constant over space and time.

In what follows, we derive an example simulation algorithm that can yield accurate current/voltage signals (as well as concentration profiles) for RRDEs. To do so, we exploit the cylindrical symmetry of the RRDE system. The model variables (concentration, velocity, electric potential) are assumed to be a function of two spatial coordinates, the distance r measured from the rotation axis and the distance z measured from the electrode surface. The method of finite volumes is applied: with planes parallel to the electrode surface, the investigated physical space is divided into n layers, and these layers—by a vertical tiling to m segments—are further divided into annulus-shaped control volumes. The symmetry axis of each control volume is the axis of rotation; **Fig. 12** shows a sketch of the simulation mesh.

The tiling of the space has to be made smooth enough so that the model variables can be considered homogeneous *inside* each control volume within a small time step Δt of the simulation. Increasing the smoothness, however, always necessitates the use of smaller Δt values (see Ref. [52] for setting an appropriate Δt) and increases the cost of calculation, which ultimately results in longer computation times. For the simulations presented here, a fine horizontal tiling (resulting in n_{bound} layers) was applied for the "boundary region" close to the electrode surface, and a coarser horizontal tiling (resulting in n_{out} layers) was applied for the space far from the electrode.

In the simulation algorithm the model variables are ordered into vectors of $n \cdot m$ length. In each iteration step we (i) realize Nernstian conditions (based on Eq. **41**) in those entries of the concentration vectors which correspond to a control volume neighboring either one of the two working electrodes; (ii) simulate the effect of mass transfer by solving a discrete version of Eqs. **(42a) and (42b)**; and (iii) estimate the uncompensated potential drop affecting the two working electrodes (this depends on the position of the reference point used for voltage measurement). Details of the calculations are given below.

Charge transfer effects

Charge transfer only affects those entries j of the $\boldsymbol{c}_{\mathrm{Ox}}$ and $\boldsymbol{c}_{\mathrm{Red}}$ vectors that correspond to control volumes neighboring either the disk or the ring electrode (see the control volumes marked by a colored hatching in **Fig. 12**). In every ith simulation step, new $c^{(i)}_{\mathrm{Ox},\,j}$ and $c^{(i)}_{\mathrm{Red},\,j}$ values are determined based on the previous values ($c^{(i-1)}_{\mathrm{Ox},\,j}$ and $c^{(i-1)}_{\mathrm{Red},\,j}$) as

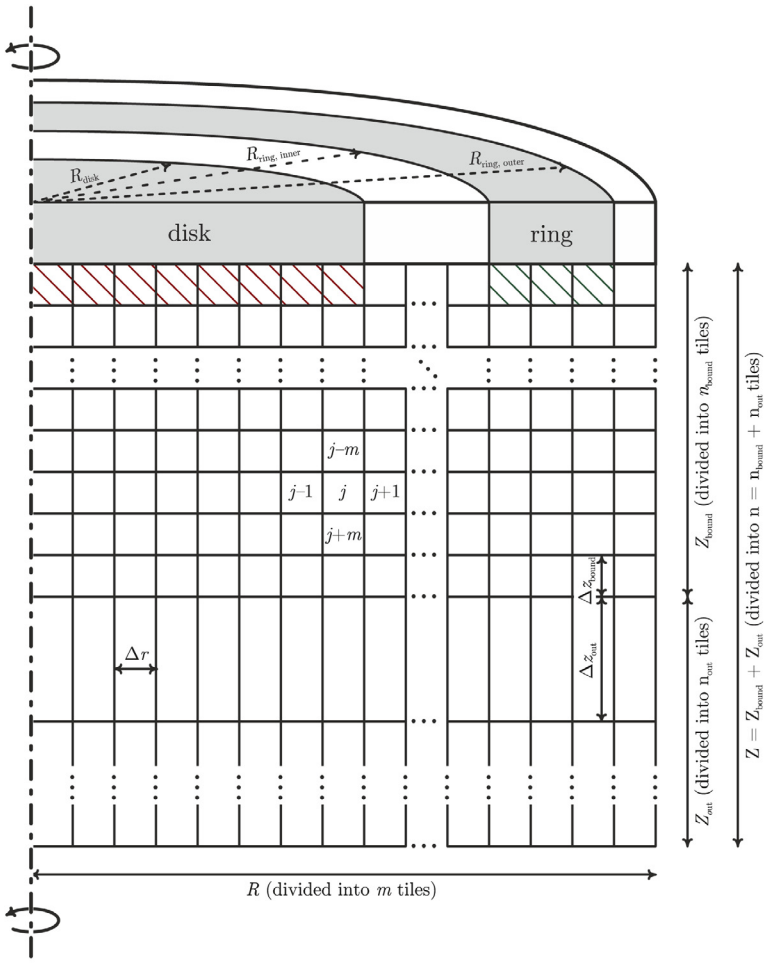

Fig. 12 Two-dimensional axi-symmetric mesh used for the spatial discretization of the RRDE system. The space below the RRDE is tiled into small annulus-shaped control volumes. The height of the volumes is smaller in the "boundary layer" close to the electrode surface; a coarser tiling is applied below this layer. *Red* and *green* hatching marks volumes which are neighboring the disk or ring electrodes, respectively. Note the rules of indexing applied: a control volume with index j can have at most four neighbors (with indices $j-1$, $j+1$, $j-m$, and $j+m$).

$$c_{\mathrm{Ox},\,j}^{(i)} = \frac{c_{\mathrm{Ox},\,j}^{(i-1)} + c_{\mathrm{Red},\,j}^{(i-1)}}{1 + \exp\left[\dfrac{\left(E^{\ominus} - \tilde{E}_{\text{disk or ring}}\right)F}{RT}\right]} \tag{43a}$$

and

$$c_{\mathrm{Red},\,j}^{(i)} = \frac{c_{\mathrm{Ox},\,j}^{(i-1)} + c_{\mathrm{Red},\,j}^{(i-1)}}{1 + \exp\left[\dfrac{\left(\tilde{E}_{\text{disk or ring}} - E^{\ominus}\right)F}{RT}\right]}, \tag{43b}$$

in accordance with the Nernst equation (42). In Eqs. **(43a) and (43b)** the $\widetilde{E}_{\text{disk or ring}}$ term is the applied potential of the working electrode neighboring the jth control volume corrected with the ohmic drop affecting the electrode in question:

$$\widetilde{E}_{\text{disk or ring}} = E_{\text{disk or ring}} - \delta_{IR,\text{disk or ring}}. \tag{44}$$

In the ith step each jth control volume (with volume V_j) that neighbors either one of the working electrodes gives an

$$I_j^{(i)} = \frac{FV_j\left(c_{\mathrm{Ox},j}^{(i)} - c_{\mathrm{Ox},j}^{(i-1)}\right)}{\Delta t} \tag{45a}$$

$$= \frac{FV_j c_{\mathrm{Ox},j}^{(i-1)} + c_{\mathrm{Red},j}^{(i-1)}}{\Delta t\left(1+\exp\left[\frac{(E^{\ominus}-\tilde{E}_{\text{disk or ring}})F}{RT}\right]\right)} - \frac{FV_j c_{\mathrm{Ox},j}^{(i-1)}}{\Delta t} \tag{45b}$$

contribution to the current of that electrode; by summing up these currents, the values of I_{disk} and I_{ring} can be determined.

The values of $\widetilde{E}_{\text{disk}}$ and $\widetilde{E}_{\text{ring}}$ are optimized in each simulation step by using a Nelder–Mead (downhill simplex[53]) root-finding algorithm. The optimum $\widetilde{E}_{\text{disk}}$ and $\widetilde{E}_{\text{ring}}$ values, when used in Eqs. (45a) and (45b), give rise to I_{disk} and I_{ring} currents which in turn establish such $\delta_{IR,\text{disk}}$ and $\delta_{IR,\text{ring}}$ values that satisfy Eq. (44). The calculation of $\delta_{IR,\text{disk}}$ and $\delta_{IR,\text{ring}}$ from I_{disk} and I_{ring} is described in detail later.

Mass transfer effects

While the electrode reactions only cause direct concentration changes in those control volumes, which are under either one of the working electrodes, mass transfer affects all the entries of the $\boldsymbol{c}_{\text{Ox}}$ and $\boldsymbol{c}_{\text{Red}}$ vectors. The general transport equations (43a)–(43b) can be rewritten in the form of a matrix-vector equation as

$$\boldsymbol{c}_{\text{Ox or Red}}^{(i)} = (\boldsymbol{II} + D_{\text{Ox or Red}}\mathrm{DD})(\boldsymbol{II} - \mathrm{VV})\boldsymbol{c}_{\text{Ox or Red}}^{(i-1)}, \tag{46}$$

where **I** is the $nm \times nm$ identity matrix and the **D** *diffusor* and **V** *conveyor* operators (also $nm \times nm$ matrices) are defined as

$$\mathbf{D}_{k,\ell} = \begin{cases} \dfrac{A_{\text{sup},k}\Delta t}{V_k d_{k,\ell}} & \textit{if } \ell = k-m \\ \dfrac{A_{\text{int},k}\Delta t}{V_k d_{k,\ell}} & \textit{if } \ell = k-1 \\ -\dfrac{\Delta t}{V_k}\left(\dfrac{A_{\text{sup},k}}{d_{k,k-m}} + \dfrac{A_{\text{int},k}}{d_{k,k-1}} + \dfrac{A_{\text{ext},k}}{d_{k,k+1}} + \dfrac{A_{\text{inf},k}}{d_{k,k+m}}\right) & \textit{if } \ell = k \\ \dfrac{A_{\text{ext},k}\Delta t}{V_k d_{k,\ell}} & \textit{if } \ell = k+1 \\ \dfrac{A_{\text{inf},k}\Delta t}{V_k d_{k,\ell}} & \textit{if } \ell = k+m \\ 0 & \text{otherwise} \end{cases} \tag{47}$$

and

$$V_{k,\ell} = \begin{cases} \dfrac{v_{r,k}\Delta t}{d_{k,\ell}} & \text{if } \ell = k-1 \\ -\Delta t\left(\dfrac{v_{r,k}}{d_{k,k-1}} + \dfrac{v_{z,k}}{d_{k,k+m}}\right) & \text{if } \ell = k \\ \dfrac{v_{z,k}\Delta t}{d_{k,\ell}} & \text{if } \ell = k+m \\ 0 & \text{otherwise} \end{cases} \tag{48}$$

In the definitions (48)–(49) $d_{k,\ell}$ denotes the distance of the centers of the kth and the ℓth control volumes; $A_{\text{sup},k}$, $A_{\text{int},k}$, $A_{\text{ext},k}$, and $A_{\text{inf},k}$ denote the superior, interior, exterior, and inferior bounding surface areas of the kth control volume with a volume of V_k; $v_{r,k}$, and $v_{z,k}$ denote, respectively, the radial and axial flow velocity components at the center point of the kth control volume.

Here we note that **D** and **V** are both large; however sparse banded matrices containing nonzero entries in only five (respectively, three) of their diagonals. Therefore, instead of storing the full matrices we only deal with their nonzero diagonals in the simulation algorithm, which gives a significant increase to the computation speed.

Provided that a smooth enough tiling is used in combination with a small Δt value, results of the simulation agree very well with basic theoretical predictions. For example, for a simple collection experiment, as shown in Fig. 13, limiting currents simulated for the disk match (usually within 0.5% of error) the predictions of the Levich equation, and there is also a good agreement ($<2\%$ of error) between simulated and theoretical collection efficiencies (the latter calculated from Eq. 7).

IR-drop-related effects

In section "Measurements With RRDEs" it was mentioned that for well-behaving RRDE systems, the current-potential characteristics of the disk should always remain unaffected by any processes that may occur on the ring electrode. If this is not the case, the reason often is an undesirable coupling of the ring and disk signals through the uncompensated solution resistance. This "electrical

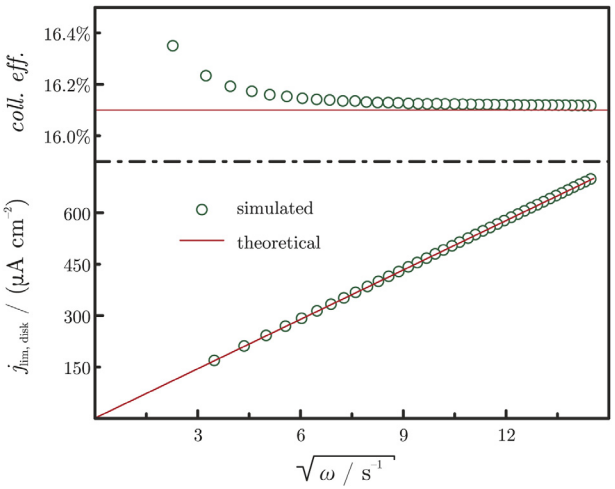

Fig. 13 Simulation results from a "steady-state collection" experiment. The disk current densities follow the Levich equation, Eq. **(1)** (lower part of the figure), while the simulated collection efficiencies are very close to their theoretical value given by Eq. **(7)**. See Ref. [52] for details and simulation settings.

cross-talk" often becomes apparent in RRDE measurements in the form of a "ghost signal" of one of the working electrodes' current, appearing superimposed on the current/voltage characteristics of the other electrode.

Cross-talk originates from the shared current routes of the two working electrodes and causes an uncompensated potential shift at one electrode, depending on the current flow of the other one. Cross-talk can, in many cases, lead to serious misinterpretations of the current signals measured in four-electrode systems; this is especially true if transient perturbations resulting in high currents are applied to either one or both of the working electrodes.

In order to implement the simulation of *IR*-drop-related cross-talk effects in our model, we interpret the simulation mesh as a network of electrical resistors, like the one shown in **Fig. 14**.

In case we have a total number of $n \cdot m$ control volumes in the simulation mesh, the "equivalent circuit" of the mesh will contain $n \cdot m + 3$ equipotential nodes, due to the three metallic conductors (the disk, the ring, and the auxiliary electrode) present in the system. The electric potentials of each node will be ordered in the vector $\boldsymbol{\psi}$ according to the following indexing rule:

- ψ_k is the electric potential corresponding to the kth control volume of the simulation mesh if $1 \leq k \leq n \cdot m$;
- ψ_k is the electric potential corresponding to the *disk* electrode if $k = n \cdot m + 1$;
- ψ_k is the electric potential corresponding to the *ring* electrode if $k = n \cdot m + 2$;
- ψ_k is the electric potential corresponding to the *auxiliary* electrode if $k = n \cdot m + 2$.

Similarly the currents leaving or entering the circuit at each node will be ordered in the vector $\boldsymbol{\iota}$. Since current cannot enter or leave the system, except through the aforementioned electrode metals, $\boldsymbol{\iota}$ will have only three nonzero entries (its last three entries), the sum of which is 0.

Regarding the conductances (inverse resistances) present in the equivalent circuit, we note the following:

- Between neighboring control volumes (with indices k and ℓ) the symmetric $\sigma_{k,\ell} = \sigma_{\ell,k}$ conductance is obtained from the constant bulk conductivity κ as

$$\sigma_{k,\ell} = \sigma_{\ell,k} = \frac{\kappa A_{k,\ell}}{d_{k,\ell}}, \tag{49}$$

  where $A_{k,\ell}$ is the bounding area between the two control volumes and $d_{k,\ell}$ is the distance of their center points.
- If a control volume with index k neighbors the disk electrode ($\ell = n \cdot m + 1$), the ring electrode ($\ell = n \cdot m + 2$) or the auxiliary electrode ($\ell = n \cdot m + 3$) then, due to the assumption that all electrode processes, is reversible,

$$\sigma_{k,\ell} = \sigma_{\ell,k} = \infty. \tag{50}$$

  In practice, usually a very high value is assumed here instead of infinity.
- If two nodes (with indices k and ℓ) are not neighbors, then

$$\sigma_{k,\ell} = \sigma_{\ell,k} = 0. \tag{51}$$

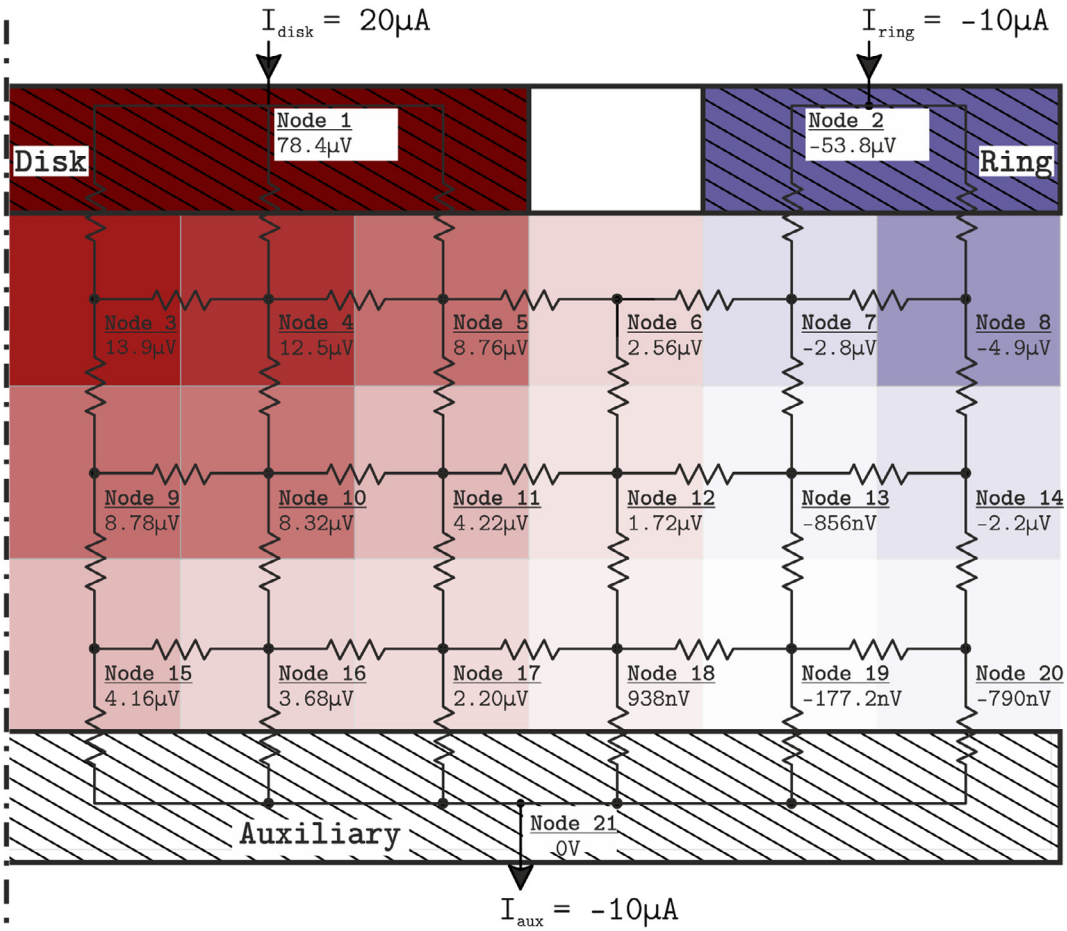

Fig. 14 Interpretation of the simulation grid as a network of electrical resistances. As an example, potential distributions have been calculated for a case when currents of opposite sign enter "Disk" and "Ring." In this illustrative calculation, the resistance values of the circuit have all been set to a value of 1 Ω, except for the resistances crossing the "Disk" or "Ring" boundary: these have a value of 10 Ω. The intensity of coloring is in accordance with the ψ value for each cell; cold colors stand for negative, and warm colors for positive potentials.

Based on the above definitions it is possible to construct the *Kirchhoff* operator **K**, an $(nm+3)\times(nm+3)$ matrix as

$$\mathrm{K}_{k,\ell}=\begin{cases}-\sigma_{k,\ell} & \text{if } \ell\neq k\\ \sum\limits_{q\neq k}\sigma_{(k,q)} & \text{if } \ell=k\end{cases} \tag{52}$$

In the context of graph theory, the Kirchhoff matrix is often alternatively called the (weighted) Laplace matrix, see Ref. [54]. In order to estimate the ohmic drop affecting the two working electrodes, the matrix-vector representation of Kirchhoff's current laws may be written as

$$\mathbf{K}\boldsymbol{\psi}=\boldsymbol{\iota}, \tag{53}$$

and Eq. (53) has to be solved for $\boldsymbol{\psi}$. Since **K** is singular, solving Eq. (53) is only possible by calculating the generalized (or Moore–Penrose) inverse[55] $\mathbf{K}^{\dagger}$, after which the vector of electric potentials can be obtained as

$$\boldsymbol{\psi}=\mathbf{K}^{\dagger}\boldsymbol{\iota}. \tag{54}$$

It is known that instead of using any (slow) iterative methods for computing the Moore–Penrose inverse, $\mathrm{K}^{\dagger}$ can also be calculated[54] directly as

$$\mathbf{K}^{\dagger}=\left(\mathbf{K}+\frac{1}{nm+3}\mathbf{J}\right)^{-1}-\frac{1}{nm+3}\mathbf{J}, \tag{55}$$

where **J** is a $(nm+3)\times(nm+3)$ matrix, all the entries of which are equal to 1. The matrix inversion in Eq. (55) is still a rather time-consuming computation; however, since the resistances in the network remain essentially unchanged during the simulation (this is a result of assuming reversible electrode reactions), it is enough to calculate $\mathbf{K}^{\dagger}$ once, only at the start of the simulations. Using the $\mathbf{K}^{\dagger}$

matrix it is then possible to obtain the $\boldsymbol{\psi}$ vector in each iteration step from Eq. (54). In Fig. 14 we show a potential field determined by the calculations outlined above, for the case when currents of opposite sign enter the "disk" and "ring" electrodes in a simplified equivalent circuit.

The vector $\boldsymbol{\psi}$ obtained from Eq. (54) is only determined up to an additive constant, which is due to the fact that $\mathbf{K}$ is a positive semidefinite matrix that has exactly one zero eigenvalue with a corresponding element-wise constant eigenvector. The $\delta_{IR,\text{disk}}$ and $\delta_{IR,\text{ring}}$ terms, which—as we will see—are responsible for the appearance of electrical cross-talk, must therefore be defined in the form of a difference:

$$\delta_{IR,\text{disk}} = \boldsymbol{\psi}_1 - \boldsymbol{\psi}_r \tag{56a}$$

$$\delta_{IR,\text{ring}} = \boldsymbol{\psi}_2 - \boldsymbol{\psi}_r, \tag{56b}$$

where r ($1 \leq r \leq nm$) is the index of the control volume chosen as the reference point for voltage measurement. Note that the above model relies on the axial symmetry of the RRDE geometry; thus "reference point" in this context means a "reference annulus-shaped simulation cell." Still, as we will show below, the reference point for voltage measurement is in practice almost equivalent to the position of the tip of a Luggin probe, and can have a very deep impact on the current–voltage characteristics of the two working electrodes.

The effect of *IR*-drop-related cross-talk, already addressed in the section "**Measurements With RRDEs**," is demonstrated in Fig. 15 where results of simulations and experiments are compared. The system studied here contained both components of a simple redox couple in the same concentration (for details, see Refs. [50,51]). Simulations and experiments both prove that the intensity and appearance of electrical cross-talk in an RRDE system depend heavily both on the overall ohmic resistance of the system (a more conductive system results in less significant cross-talk) and on the actual placement of the reference electrode.

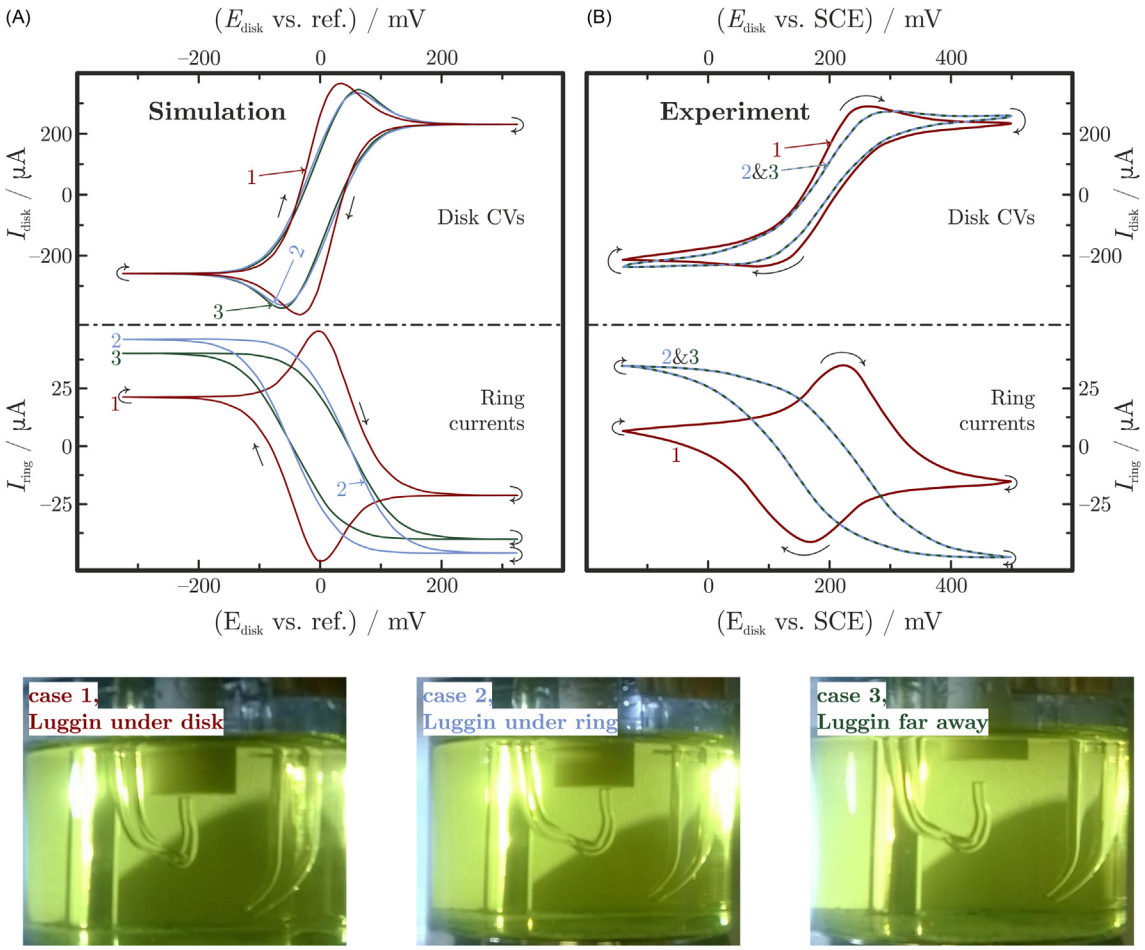

Fig. 15 Simulated (A) and measured (B) disk voltammograms and ring currents recorded in parallel with them in a system that contains a standard redox couple in equal concentrations. Cyclic voltammograms on the disk are recorded symmetrically around the equilibrium potential: the ring electrode is fixed at the equilibrium potential value. Disk sweep rate: 50 mV s^{-1}, rotation rate: 100 min^{-1}. In cases 1, 2, and 3 the Luggin probe is positioned differently under the RRDE tip, as illustrated by the photos. See Ref. [50] for details.

If the Luggin probe is set close to either one of the working electrodes, the current of that electrode gives a significant shift to the reference potential and thus to the effective potential of the other working electrode. This becomes the most obvious in case 1 in Fig. 15, where the reference point for voltage measurement is set close to the disk surface. As a result, practically no *IR*-drop will affect the disk; however the effective ring potential cannot be held stable and a "ghost signal" of the disk appears in the ring current.

Electrochemistry textbooks, when introducing the concept of *IR*-drop in a *standard three-electrode cell*, often suggest that its disturbing effect can largely be eliminated if "the reference electrode is designed for very close placement to the working electrode by use of a fine tip called a Luggin-Haber capillary".[4] In the light of what was said above it should be stressed, however, that following the very same strategy in a *four-electrode cell* (i.e., for RRDE measurements) can lead to the appearance of heavy cross-talk and can seriously complicate the interpretation of measured data.

Concluding Remarks

Rotating disk and ring–disk electrode techniques provide very useful means for the mechanistic analysis of electrode processes. In this article I attempted to give a brief and practical (yet by no means thorough) introduction to the use of these techniques, as well as to describe strategies of data analysis and modeling. I have high hopes that the readers of this book will find the chapter a good starting point for familiarizing themselves with RDE and RRDE methods.

References

1. von Helmholtz, H. L. Ueber Bewegungsströme am polarisierten Platina. *Ann. Phys.* **1880,** *247,* 737–759.
2. *Journal of Physical Chemistry* **1944**, *18,* 335–355.
3. Levich, B. The Theory of Concentration Polarization. *Discuss. Faraday Soc.* **1947,** *1,* 37–49.
4. Bard, A. J.; Faulkner, L. R. *Electrochemical Methods: Fundamentals and Applications,* 2nd ed.; John Wiley & Sons: New York, 2001.
5. Levich, V. G. *Physicochemical Hydrodynamics*, Prentice-Hall: Englewood Cliffs, NJ, 1962.
6. Riddiford, A. C. The Rotating Disk System. In *Advances in Electrochemistry and Electrochemical Engineering;* Delahay, P., Ed.; vol. 4; Interscience: New York, 1966.
7. Albery, W. J.; Hitchman, M. L. *Ring–Disc Electrodes*, Oxford University Press: London, 1971.
8. Albery, W. J. Ring–Disc Electrodes. Part 1.—A New Approach to the Theory. *Trans. Faraday Soc.* **1966,** *62,* 1915–1919.
9. Albery, W. J.; Bruckenstein, S. Ring–Disc Electrodes. Part 2.—Theoretical and Experimental Collection Efficiencies. *Trans. Faraday Soc.* **1966,** *62,* 1920–1931.
10. Albery, W. J.; Bruckenstein, S.; Napp, D. T. Ring–Disc Electrodes. Part 3.—Current-Voltage Curves at the Ring Electrode With Simultaneous Currents at the Disc Electrode. *Trans. Faraday Soc.* **1966,** *62,* 1932–1937.
11. Albery, W. J.; Bruckenstein, S.; Johnson, D. C. Ring–Disc Electrodes. Part 4.—Diffusion Layer Titration Curves. *Trans. Faraday Soc.* **1966,** *62,* 1938–1945.
12. Albery, W. J.; Bruckenstein, S. Ring–Disc Electrodes. Part 5.—First-Order Kinetic Collection Efficiencies at the Ring Electrode. *Trans. Faraday Soc.* **1966,** *62,* 1946–1954.
13. Albery, W. J.; Bruckenstein, S. Ring–Disc Electrodes. Part 6.—Second-Order Reactions. *Trans. Faraday Soc.* **1966,** *62,* 2584–2595.
14. Albery, W. J.; Bruckenstein, S. Ring–Disc Electrodes. Part 7.—Homogeneous and Heterogeneous Kinetics. *Trans. Faraday Soc.* **1966,** *62,* 2596–2606.
15. Albery, W. J. Ring–Disc Electrodes. Part 8.—Transient Currents and First-Order Kinetics. *Trans. Faraday Soc.* **1967,** *63,* 1771–1781.
16. Albery, W. J.; Hitchman, M. L.; Ulstrup, J. Ring–Disc Electrodes. Part 9.—Application to First-Order Kinetics. *Trans. Faraday Soc.* **1968,** *64,* 2831–2840.
17. Albery, W. J.; Hitchman, M. L.; Ulstrup, J. Ring–Disc Electrodes. Part 10.—Application to Second-Order Kinetics. *Trans. Faraday Soc.* **1969,** *65,* 1101–1112.
18. Albery, W. J. Ring–Disc Electrodes. Part 11.—General Theory of Transient Currents. *Trans. Faraday Soc.* **1971,** *67,* 153–160.
19. Albery, W. J.; Drury, J. S.; Hitchman, M. L. Ring–Disc Electrodes. Part 12.—Application to Ring Current Transients. *Trans. Faraday Soc.* **1971,** *67,* 161–165.
20. Albery, W. J.; Drury, J. S.; Hitchman, M. L. Ring–Disc Electrodes. Part 13.—The Laplace Transformation of Transients. *Trans. Faraday Soc.* **1971,** *67,* 166–169.
21. Albery, W. J.; Drury, J. S.; Hitchman, M. L. Ring–Disc Electrodes. Part 14.—Kinetic and Transient Parameters. *Trans. Faraday Soc.* **1971,** *67,* 2161–2166.
22. Albery, W. J.; Drury, J. S.; Hutchinson, A. P. Ring–Disc Electrodes. Part 15.—Alternating Current Measurements. *Trans. Faraday Soc.* **1971,** *67,* 2414–2418.
23. Albery, W. J.; Drury, J. S. Ring–Disc Electrodes. Part 16.—A Comparison of Analytical and Numerical Solutions. *J. Chem. Soc. Faraday Trans. 1* **1972,** *68,* 456–464.
24. Bruckenstein, S.; Tokuda, K.; Albery, W. J. Ring–Disc Electrodes. Part 17.—Ring Response to Periodic Disc Electrode Forcing Functions. *J. Chem. Soc. Faraday Trans.* **1977,** *73,* 823–829.
25. Albery, W. J.; Compton, R. G.; Hillman, A. R. Ring–Disc Electrodes. Part 18.—Collection Efficiency for High Frequency a.c. *J. Chem. Soc. Faraday Trans. 1* **1978,** *74,* 1007–1019.
26. Albery, W. J.; Hillman, A. R. Ring–Disc Electrodes. Part 19.—Adsorption Studies at Low Frequency a.c. *J. Chem. Soc. Faraday Trans. 1* **1979,** *75,* 1623–1634.
27. Albery, W. J.; Boutelle, M. G.; Colby, P. J.; Hillman, A. R. Ring–Disc Electrodes. Part 20.—A General Procedure for Deducing Faradaic Component of a Disc-Current Transient From a Ring-Current Transient. *J. Chem. Soc. Faraday Trans. 1* **1982,** *78,* 2757–2763.
28. Albery, W. J.; Calvo, E. J. Ring–Disc Electrodes. Part 21.—pH Measurement With the Ring. *J. Chem. Soc. Faraday Trans. 1* **1983,** 2583–2596.
29. Albery, W. J.; Mount, A. R. Ring–Disc Electrodes. Part 22.—Theory of the Measurement of Proton Fluxes at the Disc. *J. Chem. Soc. Faraday Trans. 1* **1989,** *85,* 1181–1188.
30. Albery, W. J.; Mount, A. R. Ring–Disc Electrodes. Part 23.—Studies of Proton Fluxes at a Thionine-Coated Electrode. *J. Chem. Soc. Faraday Trans. 1* **1989,** *85,* 1189–1198.
31. Albery, W. J.; Mount, A. R. Ring–Disc Electrodes. Part 24.—Studies of Counterion Fluxes at a Thionine-Coated Electrode. *J. Chem. Soc. Faraday Trans. 1* **1989,** *85,* 3717–3724.
32. Grozovski, V.; Vesztergom, S.; Láng, G. G.; Broekmann, P. Electrochemical Hydrogen Evolution: H^+ or H_2O Reduction? A Rotating Disk Electrode Study. *J. Electrochem. Soc.* **2017,** *164,* 3171–3178.
33. A. Rudnev, Y.-Ch. Fu, I. Gjuroski, F. Stricker, J. Furrer, N. Kovács, S. Vesztergom, P. Broekmann, Transport Matters: Boosting CO_2 Electroreduction in [BMIm][BF4]/Water Mixtures by Enhanced Diffusion. *ChemPhysChem.* Vol. 22, pp. 3153–3162.
34. Frumkin, A. N.; Nekrasov, L. N.; Levich, V. G.; Ivanov, Y. B. Die Anwendung der rotierenden Scheibenelektrode mit einem Ringe zur Untersuchung von Zwischenprodukten elektrochemischer Reaktionen. *J. Electroanal. Chem.* **1959,** *1,* 84–89.
35. Shabrang, M.; Bruckenstein, S. Equivalent Circuit for the Uncompensated Resistances Occurring at Ring–Disk Electrodes. *J. Electrochem. Soc.* **1974,** *121,* 1439–1444.
36. Dörfel, C.; Rahner, D.; Forker, W. Studies of Coupling Effects and Ohmic Potential Drops at Ring-Disc Electrodes. *J. Electroanal. Chem.* **1980,** *107,* 257–270.
37. Trinh, D.; Maisonhaute, E.; Vivier, V. Electrical Cross-Talk in Transient Mode of Scanning Electrochemical Microscopy. *Electrochem. Commun.* **2012,** *16,* 49–52.
38. Pine Instruments Company, Operating Instructions for AFRDE5 Potentiostat, Grove City PA, 1992.
39. ZAHNER-Elektrik GmbH & Co.KG, External Potentiostats Installation and Operation Manual, Kronach, 2010.

40. Cadle, S. H.; Bruckenstein, S. Ring–Disk Electrode Study of the Anodic Behavior of Gold in 0.2M Sulfuric Acid. *Anal. Chem.* **1974,** *46,* 16–20.
41. Vesztergom, S.; Ujvári, M.; Láng, G. G. RRDE Experiments With Potential Scans at the Ring and Disk Electrodes. *Electrochem. Commun.* **2011,** *13,* 378–381.
42. Vesztergom, S.; Ujvári, M.; Láng, G. G. Dual Cyclic Voltammetry With Rotating Ring–Disk Electrodes. *Electrochim. Acta* **2013,** *110,* 49–55.
43. Kamar, E. M.; Miller, B. Electrochemical Behavior of La_2CuO_4 in Aqueous Media. *J. Electrochem. Soc.* **1999,** *146,* 1862–1865.
44. Vesztergom, S.; Kovács, N.; Ujvári, M.; Láng, G. G. Apparatus and Methods for Using a Rotating Ring–Disk Electrode With Potentiodynamic Control of Both Working Electrodes. *Technisches Messen* **2017,** *84,* 683–696.
45. Vesztergom, S.; Ujvári, M.; Láng, G. G. RRDE Experiments With Independent Potential Scans at the Ring and Disk Electrodes—3D Map of Intermediates and Products of Electrode Processes. *Electrochem. Commun.* **2012,** *19,* 1–4.
46. von Kármán, T. Über laminare und turbulente Reibung. *Zeitschrift für Angewandte Mathematik und Mechanik* **1921,** *1,* 233–252.
47. Cochran, W. G. The Flow Due to a Rotating Disc. *Math. Proc. Cambridge Philos. Soc.* **1934,** *30,* 365–375.
48. Prater, K. B.; Bard, A. J. Rotating Ring–Disk Electrodes I. Fundamentals of the Digital Simulation Approach. Disk and Ring Transients and Collection Efficiencies. *J. Electrochem. Soc.* **1970,** *117,* 207–213.
49. Feldberg, S. W.; Bowers, M. L.; Anson, F. C. Hopscotch-Finite-Difference Simulation of the Rotating Ring–Disc Electrode. *J. Electroanal. Chem. Interfacial Electrochem.* **1986,** *215,* 11–28.
50. Vesztergom, S.; Barankai, N.; Kovács, N.; Ujvári, M.; Siegenthaler, H.; Broekmann, P.; Láng, G. G. Electrical Cross-Talk in Rotating Ring–Disk Experiments. *Electrochem. Commun.* **2016,** *68,* 54–58.
51. Vesztergom, S.; Barankai, N.; Kovács, N.; Ujvári, M.; Siegenthaler, H.; Broekmann, P.; Láng, G. G. Electrical Cross-Talk in Four-Electrode Experiments. *J. Solid State Electrochem.* **2016,** *20,* 3165–3177.
52. Vesztergom, S.; Barankai, N.; Kovács, N.; Ujvári, M.; Wandlowski, T.; Láng, G. G. Rotating Ring–Disk Electrode With Dual Dynamic Potential Control: Theory and Practice. *Acta Chim. Slov.* **2014,** *61,* 223–232.
53. Nelder, J. A.; Mead, R. A Simplex Method for Function Minimization. *Comput. J.* **1965,** *7,* 308–313.
54. Gutman, I.; Xiao, W. Generalized Inverse of the Laplacian Matrix and Some Applications. *Bulletin d'Académie serbe des sciences et des arts. Classe des sciences mathématiques et naturelles. Sciences mathématiques* **2004,** *29,* 15–23.
55. Ben-Israel, A.; Greville, T. N. E. *Generalized Inverses. Theory and Applications*, Springer: Heidelberg, 2003.